Lawrence Berkeley Laboratory
UNIVERSITY OF CALIFORNIA

ENERGY & ENVIRONMENT
DIVISION

ON CONVECTIVE HEAT TRANSFER IN BUILDING ENERGY ANALYSIS

Ashok Jagannath Gadgil
(Ph.D. thesis)

May 1980

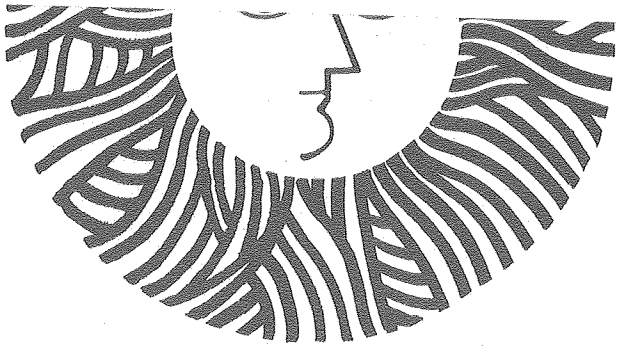

Prepared for the U.S. Department of Energy under Contract W-7405-ENG-48

DISCLAIMER

To My Parents

TABLE OF CONTENTS

ACKNOWLEDGMENTS

This thesis concludes three years of research with the Passive Solar Group at Lawrence Berkeley Laboratory and the Physics Department at U.C.Berkeley. I wish to extend my warmest thanks to the faculty and to the staff of the Solar Group for their support. I would like to acknowledge personally the specific contributions by a number of people to this research.

My work on developing the building model TWOZONE, initiated by Art Rosenfeld and Ed Dean, introduced me to the field of building energy analysis four years ago. Discussions with Leonard Wall and Tom Borgers, both of whom were spending their sabbaticals at LBL, were helpful in getting me started on my thesis problem. Hashem Akbari, presently teaching in Iran, took a keen interest in the progress of this work. Numerous discussions with him have been of great help in clarifying my ideas at several stages of this thesis. I can only offer my warmest gratitude for his relentless concern for my work.

Ron Kammerud went through an early draft of the thesis and his critical comments have improved the readability of this paper considerably. His patient support in the early stages of the work when no results were forthcoming, and his hard-nosed interest in validation of this model must be gratefully mentioned. Members of my Thesis Committee, Paul Condon and Ed Dean provided thoughtful comments on the extent and exposition of this work. I wish to express thanks for helpful discussions with Prof. R. Greif and Prof. S. V. Patankar of the Mechanical Engineering Departments of U.C.Berkeley and University of Minnesota respectively.

Cindy Polansky typed the early drafts; the final draft was typed fast and accurately by Deberah Craig. The drawings were done by Jesse Goodlow.

This work was supported by the Solar Heating and Cooling Research and Development Branch, Office of Conservation and Solar Applications, U.S. Department of Energy, under contract number W-7405-ENG-48.

My thanks to Anjali, my wife, cannot be expressed in this formal manner. I would like to mention here that without her cheerful encouragement and patience, this project wouldn't have been finished.

ON CONVECTIVE HEAT TRANSFER IN BUILDING ENERGY ANALYSIS

Ashok Jagannath Gadgil

Passive Solar Group, Energy and Environment Division
Lawrence Berkeley Laboratory
University of California
Berkeley, California 94720

ABSTRACT

In the ongoing efforts to study energy consumption in buildings through computer simulations, practically no attention has been given to modeling natural convective heat transfer in buildings. The main reason for this neglect is due to the difficulty of solving the problem numerically. This paper makes a contribution towards the solution of this difficulty by presenting a numerical code for modeling natural convection in rectangular enclosures at Rayleigh numbers up to 10^{10}.

Chapter 2 develops the general equations of motion to be solved.

Chapter 3 is devoted to simplification of these equations and description of the numerical scheme.

Chapter 4 describes the comparisons of the predictions of the computer program based on the numerical scheme with various published experimental and numerical results of other investigators.

Chapter 5 illustrates an application of the computer program to investigate the soundness of an assumption commonly made by all the building energy analysis programs.

CHAPTER 1

INTRODUCTION

1.1 The Relevance of Building Energy Physics

After the onset of the so-called energy crisis since 1973, attention of many energy strategists in the U.S. has been focused on the energy used for heating and cooling of the interior of buildings. This energy consumption, commonly referred to as energy consumption for space conditioning, constitutes about 20% of the total energy consumption of 75 quads per year (1 quad = 10^{15} Btu $\cong 3 \times 10^{11}$ kwh) in the U.S. today.

Space conditioning has been an area of high total energy use and low optimization of design and construction with respect to energy use. Naturally, the last few years have seen many keen minds turning to this relatively unexplored field.

The problem is not new. It has already been faced in Europe, where the cost of energy was already much higher and the energy situation precarious in many countries. This is reflected, for example, in the attention being given to the problems of heat transfer inside buildings by academic researchers in Europe earlier than in the U.S. (e.g., Ref. 1,2).

1.2 Modeling Energy Flows in Buildings

In the U.S., the first modern public domain computer code for analysis of the thermal behavior of buildings was written in the late 1960s for the U.S. government called NECAP (Ref. 3). This was soon followed by Cal-ERDA and DOE-1 computer programs (Refs. 4,5). All three

programs used response factor methods to calculate heat flow through user-defined multi-layered walls and user-defined windows. The computer program NBSLD (Ref. 6) developed at the National Bureau of Standards, calculated detailed radiative heat transfers between interior surfaces by performing a detailed thermal balance calculation for each pair of surfaces, in addition to solving for heat conduction through multi-layered walls as done by DOE-2. BLAST (Ref. 7), developed at the Civil Engineering Research Laboratory of the U.S. Army, has carried the state of the art further by improving on the architecture, speed and accuracy of NBSLD. (For a comparison of some of these programs, see Refs. 8,9).

In parallel with the development of these numerical models of energy flows inside buildings, there also have been attempts to develop analytical models of building energy flows (Refs. 10,11). These models have been successful in their limited domain defined by the analytical assumptions made by their authors, but the assumptions have been constraining enough to invalidate wide application.

All the building models referred to above have various degrees of sophistication in the treatment of conductive and radiative heat transfers (the most sophisticated, at this time, is BLAST-2.0). However, in the treatment of convective heat transfer, all these models are rather simplistic. This is not due to some oversight on the part of the designers of these models; rather it stems from the extreme complexity of the problem involved. The net result of the difficulty of modeling convective energy flows in buildings has been that though the radiative and convective heat transfer mechanisms are roughly of equal magnitude in a real house, the more advanced building models have become increasingly sophisticated in

radiation modeling, leaving convective modeling for later. (BLAST-2.0 does allow, for example, user-defined, variable convective heat transfer coefficients from surfaces, but it cannot tell you what heat transfer coefficients to use.)

There have been both experimental and theoretical attempts to understand convective energy flows in buildings under a variety of specific situations. Ruberg (Ref. 12) has experimentally investigated the convective flow in a full-scale test chamber. Casperson and Hocevar (Ref. 13) and Akbari and Borgers (Ref. 14) have carried out detailed experimental and numerical investigations of flow in a Trombe wall channel. Burns, Chow and Tien (Ref. 15) have investigated numerically the effect of air infiltration through cracks in an insulation-filled wall. Balcomb's group at LASL has carried out experiments on several solar strategies by instrumenting test cells (Ref. 16). Weber and Wray (Ref. 17) have recently reported on detailed experimental investigation of convective energy flow in a scaled model of two zones connected by a doorway.

Development of a general three-dimensional computer model of convective energy flow is the next logical step towards better understanding and better design of buildings, particularly passive solar buildings. It is enough to point to the unfortunate abundance of rather naive "thermal flow diagrams" for various passive solar houses (see Ref. 18) to be convinced of the state of ignorance regarding convective energy flows in buildings. Some practicing architects and investigators almost seem to think that in a real house air will flow along directions which they have chosen to indicate by arrows in their design — often against the laws of physics.

The following pages describe the construction and validation of a computer code for modeling buoyancy-driven convective air flow in a rectangular shaped enclosure using the formulation proposed by Spalding (Ref. 19). The code can be modified to incorporate more complex geometries.

CHAPTER 2

THE GOVERNING EQUATIONS

2.1 Introduction

To understand the behavior of air movement inside a building, one must first formulate, in general, the laws of motion which govern the movement of air. Applying these laws of motion to air flow under the specific boundary conditions (surface temperatures, any inlets or outlets for air streams, etc.) encountered in the situation of interest will, in principle, define the problem completely. We say "in principle" because as we will see below, the equations of motion governing the air flow are very hard to solve analytically. And even with numerical techniques using modern large computers, solutions are not obtainable under any arbitrary conditions. In this chapter, the general equations which govern fluid flow are developed and described. Assumptions appropriate to the specific class of problems of interest herein are presented and the resulting simplified laws of motion are cast into a form suitable for numerical solution.

2.2 The Navier Stokes Equations

The full equations governing the flow of a fluid are known as the Navier-Stokes equations. Each of them is discussed below. The notation and the choice of axes are shown in Fig. 1.

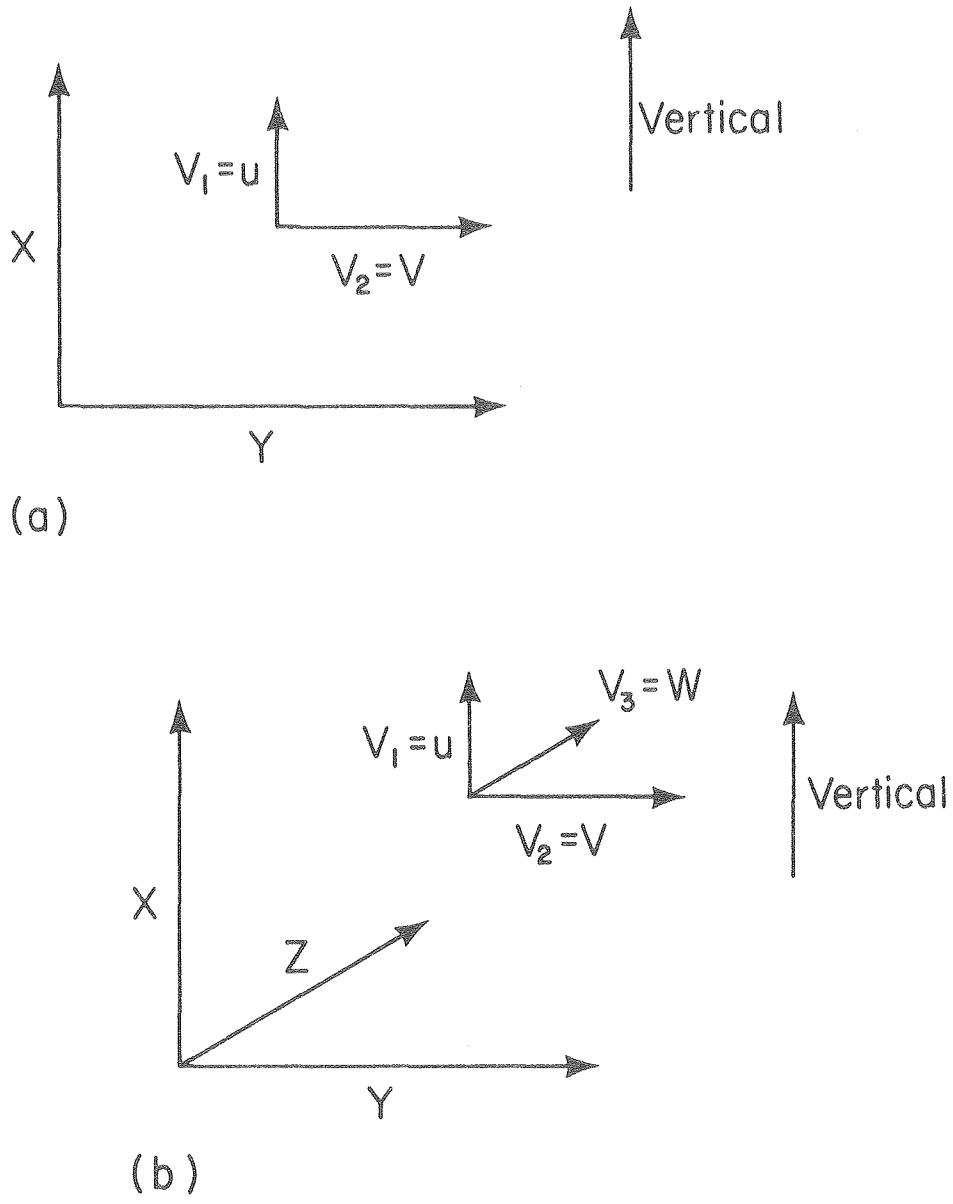

Fig 1. THE COORDINATE AXES AND VELOCITY COMPONENTS AS USED IN THE TEXT AND FIGURES, FOR TWO AND THREE DIMENSIONS.

XBL7911-13115

A. Conservation of Mass

Conservation of mass is expressed by the equation:

$$\frac{\partial \rho}{\partial t} + \text{div}\,(\rho \vec{V}) = 0 \quad . \tag{2.1}$$

The physical significance of each of the two terms in the equation can be obtained by integrating this equation over an elementary infinitesimal volume. The first term gives the time derivative of the net mass of fluid contained in the volume, while the second term, changed to a surface integral using Gauss's theorem, gives the net flow of mass out of boundaries enclosing the elementary volume. The two terms must always add to zero if no fluid mass is created or destroyed within the volume.

B. Conservation of Momentum

As applied to the "point articles" and other classical solid bodies, conservation of momentum is expressed by Newton's law

$$\vec{F} = \frac{d}{dt}(m\vec{V})$$

where $\vec{F}$ is the force acting on the point in space and $\vec{V}$ is the instantaneous velocity of the particle or solid body at that point.

When dealing with continuous media, however, one must distinguish between two "kinds" of velocities: one is the velocity of a fluid element, an infinitesimal volume of fluid, as it moves around in space; the other is the local fluid velocity, defined as the fluid velocity at a specific point in space. For example, though the water in a waterfall is accelerating under gravity, the local velocity of water at a fixed point in the waterfall (fixed with respect to the earth) is obviously constant. Thus

one must move along with the fluid (air inside a room, water in the waterfall) to evaluate the acceleration of the fluid. This is accomplished with the total derivative:

$$\frac{d}{dt} = \frac{\partial}{\partial t} + \frac{dx}{dt}\frac{\partial}{\partial x} + \frac{dy}{dt}\frac{\partial}{\partial y} + \frac{dz}{dt}\frac{\partial}{\partial z}$$

where dx/dt, dy/dt, and dz/dt are the three components of the fluid velocity at the point of interest. In vector notation:

$$\frac{d}{dt} = \frac{\partial}{\partial t} + \vec{V} \cdot \text{grad} \quad .$$

The momentum balance equations for an ideal fluid (incompressible and non-viscous) can therefore be written as:

$$\rho\left[\frac{\partial \vec{V}}{\partial t} + (\vec{V} \cdot \text{grad})\vec{V}\right] = -\text{grad } P + \rho\vec{F} \qquad (2.2)$$

where the first term on the right-hand side is the force arising from the pressure gradient, and the second term, commonly called the body-force term, represents all other forces acting on the fluid. In the case under study, this term will account for buoyancy forces.

Expressing Eq. (2.2) in different terms will simplify some of the formulations introduced in Chapter 3. We rewrite Eq. (2.2) as:

$$\frac{\partial}{\partial t}(\rho\vec{V}) = -(\vec{V} \cdot \text{grad})\rho\vec{V} - \text{grad } P + \rho\vec{F} \quad . \qquad (2.2a)$$

The last two terms on the right-hand side are unchanged. The left-hand side can now be viewed as the rate of change of <u>local</u> fluid momentum; i.e., the rate of change of momentum contained in an infinitesimal volume of space around the point of interest, which is fixed with respect to the coordinate axes. The x-component, for example, of the first term on the

right-hand side is

$$V_x \frac{\partial(\rho V_x)}{\partial x} + V_y \frac{\partial(\rho V_x)}{\partial y} + V_z \frac{\partial(\rho V_x)}{\partial z} \quad .$$

This term is equal to the net amount of x-momentum convected out of the infinitesimal volume surrounding the point of observation, fixed with respect to the coordinate axes. This identification of the term $(\vec{V} \cdot \text{grad})$ as representing convective flux of a variable will be useful later.

Real fluids are neither incompressible nor non-viscous. To incorporate the effects of viscosity, one must rewrite the momentum balance equation (2.2) without the body-force term as:

$$\frac{\partial}{\partial t}(\rho V_i) = -\frac{\partial \Pi_{ik}}{\partial x_k} \tag{2.3}$$

where we define Π_{ik} as the momentum flux density:

$$\Pi_{ik} = P\delta_{ik} + \rho V_i V_k \quad . \tag{2.4}$$

Π_{ik} is the ith component of momentum entering the infinitesimal surface set up perpendicular to the kth axis; this can be immediately verified by performing volume integration on Eq. (2.3) and using Gauss's law to reduce the resulting right-hand side to a surface integral.

Viscosity is the macroscopic result of molecular process; therefore any correct modification of the momentum equations (2.2) to include the phenomenon of viscosity must proceed from micro-molecular arguments of kinetic theory (see e.g. Ref. 20), although less rigorous phenomenological arguments of macrophysics lead to correct equations and are generally considered adequate for the problem under discussion.

Viscosity effects can be included in the momentum expression by writing the most general expression that can be incorporated into Eq. (2.3), which satisfies the following phenomenologic requirements:

1) The viscous force on any fluid element at any point is proportional to the space gradient of fluid velocity at that point (Newtonian fluids).
2) The viscous force vanishes when the fluid is at rest.
3) Fluid in uniform rotation should not experience any viscous force.

The most general tensor expression satisfying these properties, which can be added to Eq. (2.4), is

$$\sigma_{ik} = a\left(\frac{\partial V_i}{\partial X_k} + \frac{\partial V_k}{\partial X_i}\right) + b\,\frac{\partial V_\ell}{\partial X_\ell}\,\delta_{ik} \qquad (2.5a)$$

where V_1, V_2 and V_3 are the velocity components along the orthogonal coordinates X_1, X_2 and X_3; a and b are coefficients and the summation convention is assumed. For an isotropic homogeneous fluid, a and b are constants.

Equation (2.5a) can be put in more familiar form by defining two constants, μ and ζ

$$\mu = -a \qquad ; \qquad \zeta = -\left(\frac{2}{3}\,a + b\right) \quad .$$

In terms of these constants, (2.5a) becomes:

$$\sigma_{ik} = -\mu\left(\frac{\partial V_i}{\partial X_k} + \frac{\partial V_k}{\partial X_i} - \frac{2}{3}\,\delta_{ik}\,\frac{\partial V_\ell}{\partial X_\ell}\right) - \zeta\delta_{ik}\,\frac{\partial V_\ell}{\partial X_\ell} \qquad (2.5b)$$

μ and ζ are called the first and second coefficients of viscosity

respectively.

The coefficient of μ is the viscous tangential force acting in direction i on the face perpendicular to direction k. Note that the coefficient is traceless (the sum of diagonal elements is zero). The coefficient of ζ is the viscous force on face i, in the direction i, due to expansion/contraction of the volume element; it is proportional to the divergence of the velocity. ζ, the second viscosity coefficient, is sometimes called the viscosity coefficient for dilatation.

With the expression (2.5b) added, the momentum flux density Π_{ik} of Eq. (2.4) now becomes

$$\Pi_{ik} = \left(p - \zeta \frac{\partial V_\ell}{\partial X_\ell}\right)\delta_{ik} + \rho V_i V_k - \mu\left(\frac{\partial V_i}{\partial X_k} + \frac{\partial V_k}{\partial X_i} - \frac{2}{3}\delta_{ik}\frac{\partial V_\ell}{\partial X_\ell}\right) . \quad (2.6)$$

For the problem under discussion, μ and ζ can be considered constants (independent of position and time). With this approximation, the momentum equation (2.3) for the ith component of velocity is:

$$\frac{\partial}{\partial t}(\rho V_i) = -\frac{\partial}{\partial X_k}(p\delta_{ik}) - \rho V_k \frac{\partial V_i}{\partial X_k} + \mu \frac{\partial^2 V_i}{\partial X_k \partial X_k}$$
$$+ \left(\zeta + \frac{\mu}{3}\right)\frac{\partial}{\partial X_k}\left(\frac{\partial V_\ell}{\partial X_\ell}\right)\delta_{ik} - V_i\left(V_k \frac{\partial \rho}{\partial X_k} + \rho \frac{\partial V_k}{\partial X_k}\right) . \quad (2.7)$$

The presence of an external body force acting on the fluid is accounted for by adding a term ρF_i to the right-hand side of Eq. (2.7). After moving the second term on the right-hand side of (2.7) to the left-hand side, and using the continuity equation (2.1) on the last term of the right-hand side, Eq. (2.7), with the term representing external force $\vec{F}$, can be written in vector form as:

$$\rho \frac{d\vec{V}}{dt} = -\text{grad } P + \rho\vec{F} + \mu\nabla^2\vec{V} + \left(\zeta + \frac{\mu}{3}\right) \text{grad} \cdot \text{div } \vec{V} \qquad (2.8a)$$

or

$$\frac{d\vec{V}}{dt} = -\frac{1}{\rho} \text{grad } P + \vec{F} + \nu\nabla^2\vec{V} + \frac{\zeta + \frac{\mu}{3}}{\rho} \text{grad} \cdot \text{div } \vec{V} \qquad (2.8b)$$

where we define $\nu = \mu/\rho$ as the kinematic viscosity.

C. The Energy Equation

The energy equation refers to combined conductive-convective heat transfer in the fluid, including the generation of heat (which will be shown to be negligible in the present case) due to viscous dissipation of mechanical energy of the fluid.

The terms representing heat generation due to viscous dissipation can be evaluated most simply as follows. We consider the expression for the rate of change of kinetic energy, $\partial/\partial t\,(\frac{1}{2}\rho V^2)$, where Eq. (2.7) is used in the rearrangement of terms. This expression, when integrated over the volume, gives the rate of change of kinetic energy of the fluid contained in the volume. If the volume is bounded by rigid boundaries, one of the two terms in the volume integral, when reduced to a surface integral by Gauss's law, disappears since the velocities vanish at the boundaries. The second term, representing the viscous dissipation of kinetic energy (and which is equal to the gain in thermal energy due to viscous dissipation) is given by

$$\frac{dq}{dt} = \mu\left(\frac{\partial V_i}{\partial X_k} + \frac{\partial V_k}{\partial X_i}\right)\frac{\partial V_i}{\partial X_k} + \left(\zeta - \frac{2\mu}{3}\right)\left(\frac{\partial V_\ell}{\partial X_\ell}\right)^2 \quad . \qquad (2.9)$$

The other two terms in the (thermal) energy equation represent the effects of conduction (diffusion) and convection. To a good approximation the thermal conductivity of air, k, can be considered to be a constant for typical conditions under study (a change of less than 0.3% in thermal conductivity per °C at room conditions). For example, temperatures within a particular enclosure might vary by 20°C at any time; the conductivity varies by less than 6% over the enclosed volume. The contribution of the conduction term to the temperature equation is given by the well-known diffusion equation

$$\rho C_p \frac{\partial T}{\partial t} = -k\nabla^2 T \quad ,$$

where C_p is the heat capacity at constant pressure and T is the temperature. The contribution from the convective process, as discussed near Eq. (2.2), is through additional terms which account for the fact that the fluid is in motion.

Thus the full equation for temperature (commonly called the energy equation) includes the conductive, convective, and viscous components and is written

$$\frac{\partial T}{\partial t} + (\vec{V} \cdot \text{grad})T = \frac{k}{\rho C_p} \nabla^2 T + \frac{\mu}{\rho C_p} \left(\frac{\partial V_i}{\partial X_k} + \frac{\partial V_k}{\partial X_i} \right) \frac{\partial V_i}{\partial X_k}$$

$$+ \frac{1}{\rho C_p} \left(\zeta - \frac{2\mu}{3} \right) \left(\frac{\partial V_\ell}{\partial X_\ell} \right)^2 \quad . \tag{2.10}$$

It will be argued that the last two terms on the right-hand side, which account for viscous dissipation, can be neglected to a very good approximation.

D. Some Simplifications of the Governing Equations

Thus the three equations governing the flow of air for the problem under consideration are commonly known as the Navier-Stokes equations; they are summarized below:

Continuity equation :

$$\frac{\partial \rho}{\partial t} + \text{div}(\rho \vec{V}) = 0 \quad , \tag{2.11a}$$

Momentum conservation :

$$\frac{\partial \vec{V}}{\partial t} + (\vec{V} \cdot \text{grad})\vec{V} = -\frac{1}{\rho} \text{grad } p + \vec{F} + \mu \nabla^2 V + \left(\frac{\zeta + \frac{\mu}{3}}{\rho} \right) \text{grad} \cdot \text{div } \vec{V} \tag{2.11b}$$

Energy equation :

$$\frac{\partial T}{\partial t} + (\vec{V} \cdot \text{grad})T = \frac{k}{\rho C} \nabla^2 T + \frac{\mu}{\rho C_p} \left(\frac{\partial V_i}{\partial X_k} + \frac{\partial V_k}{\partial X_i} \right) \frac{\partial V_i}{\partial X_k} + \frac{1}{\rho C_p} \left(\zeta - \frac{2\mu}{3} \right) \left(\frac{\partial V_\ell}{\partial X_\ell} \right)^2 \tag{2.11c}$$

The following comments on Eq. (2.11) should be considered:

(a) In the specific class of problems being considered here, many terms can be neglected in order to simplify the task of obtaining a solution. The necessary assumptions and the limitations they impose on the generality of the solutions will be discussed in Chapter 3.

(b) The variables appearing in the equations are dimensional variables (defined in terms of mass, length and time, in a specific

system of units such as the MKS or the FPS system). This is a disadvantage if one were to attempt to bring out the similarity between two different physical situations that differ from each other only by a set of scaling factors. Under such situations, if the boundary conditions and the variables appearing in the equations are properly scaled, the two problems will appear identical in terms of the numerical solution required, if the equations were set up to deal with non-dimensional variables. Seen another way, if the equations are expressed in terms of non-dimensional variables, then a specific particular solution obtained for a given set of non-dimensionally expressed boundary conditions can be readily applied to several different physical situations, by dimensionalizing the particular numerical solution with appropriate dimensionalizing parameters.

(c) The body force term $\vec{F}$ in the momentum equation represents gravitational force in the problem under study. The gravitational force for an enclosed body of fluid with constant density is balanced by a pressure gradient perfectly counteracting this force. In such a case, the gravitational force does not give rise to any fluid motion. For the problem under study, however, local changes in density (due to thermal expansion) cause unbalanced forces in the fluid that cannot, in general, be cancelled with any possible pressure configuration.*

*The force field $\vec{F}_p$ set up due to the pressure field is conservative (curl $\vec{F}_p = 0$) since this force field is simply the negative gradient of the pressure field ($\vec{F}_p$ = -grad p). This field can never cancel a non-conservative (curl $\vec{F}_b \neq 0$) body force field. The unbalanced gravitational forces due to local changes in density are in general such a non-conservative force field and so cannot be balanced by any pressure field, always giving rise to buoyant motion.

If the temperature coefficient of volume expansion at constant pressure is expressed as β (in units of temp^{-1}), the force $\vec{F}$ in the momentum equation (2.11b) can be written as

$$\vec{F} = (1 - \beta\Delta T)\vec{g} \quad , \tag{2.12}$$

where ΔT is the deviation of the local temperature from some conveniently chosen base temperature.

For the case under study, Eqs. (2.11) can be simplified since the density, temperature, and pressure are not expected to have large excursions relative to their mean values. We define the new variables P_1, T_1, and ρ_1 in terms of the old variables P, T, and ρ by the following relations:

$$P = P_0 + P_1$$

$$T = T_0 + T_1$$

$$\rho = \rho_0 + \rho_1 \quad ,$$

where P_0, T_0, and ρ_0 are constants. Restricting attention to the cases where $P_1/P_0 << 1$ and $\rho_1/\rho_0 << 1$ and $T_1/T_0 << 1$, and using the relation (2.12) in the momentum equation (2.11b), Eqs. (2.11) simplify to:

Continuity :

$$\frac{\partial \rho_1}{\partial t} + \rho_0 \, \mathrm{div}(\vec{V}) = 0 \quad , \tag{2.13a}$$

Momentum :

$$\frac{\partial \vec{V}}{\partial t} + (\vec{V} \cdot \mathrm{grad})\vec{V} = \nu\nabla^2\vec{V} - \frac{1}{\rho_0} \mathrm{grad}\, P_1 - \beta T_1 \, g\hat{i}$$

$$+ \frac{1}{\rho_0}\left(\zeta + \frac{\mu}{3}\right) \mathrm{grad} \cdot \mathrm{div}\, \vec{V} \quad , \tag{2.13b}$$

Energy :

$$\frac{\partial T_1}{\partial t} + (\vec{V}\cdot\text{grad})T_1 = \alpha\nabla^2 T_1 + \frac{\mu}{\rho_0 C_p}\left(\frac{\partial V_i}{\partial X_k} + \frac{\partial V_k}{\partial X_i}\right)\frac{\partial V_i}{\partial X_k} + \frac{1}{\rho_0 C_p}\left(\zeta - \frac{2\mu}{3}\right)\left(\frac{\partial V_\ell}{\partial X_\ell}\right)^2 \quad . \tag{2.13c}$$

where in Eq. (2.13c), α is defined as $\alpha \equiv k/\rho_0 C_p$, and where $\hat{i}$ in Eq. (2.13b) is the unit vector in the vertical direction.

The similarity between Eqs. (2.13b) and (2.13c) is not quite noticeable with regard to their left-hand sides, and also for the first terms on the right-hand sides. The similarity arises due to the fact that both equations describe convective-diffuse transport (of momentum or energy) together with various source terms on the right-hand side.

Viscosity, like thermal conduction, is a molecular transport phenomena, arising out of molecular motion. Thus the coefficients ν and α in Eqs. (2.11b) and (2.11c) are, respectively, called the momentum diffusivity (or kinematic viscosity) and thermal diffusivity.

So the second terms on the left-hand side of Eqs. (2.13b) and (2.13c) describe the convective transport, while the first terms on the right-hand side of these equations describe the diffusive transport of the particular quantity under consideration.

Equations (2.13) will be reduced to dimensionless form for reasons described in comment (b) above. The variables are rendered dimensionless by multiplying or dividing them with appropriately chosen combinations of dimensional constants. The following set of dimensional constants is used herein:

ρ_0 = Average density of air (ML^{-3}).

ν = Kinematic viscosity of air, at room temperature and atmospheric pressure (L^2T^{-1}).

b = A length-scale chosen to be characteristic for the problem. This can be, say, a length of the order of the height of a typical room (L).

Various combinations of the above three constants can be chosen to yield any desired dimension in terms of mass, length and time. In addition, a temperature constant is needed:

ΔT_0 = A temperature difference chosen to be characteristic for the problem. This can be chosen to be the difference between the maximum and minimum of the (specified) surface temperature boundary conditions.

These four constants form a complete set spanning the space of mass, length, time, and temperature. An additional constant, Δt_0, representing a time interval is also defined; this apparently redundant constant is introduced simply for later convenience.

The following dimensionless variables are defined in terms of the old dimensional variables and the five dimensional constants introduced above. The dimensionless lengths (along the three axes) are defined by:

$$X = \frac{x}{b} \quad ; \qquad Y = \frac{y}{b} \quad ; \qquad Z = \frac{z}{b} \quad .$$

The dimensionless velocity components (along the three axes) are defined by:

$$U = u\frac{b}{\nu} = V_1\frac{b}{\nu}$$

$$V = v\frac{b}{\nu} = V_2\frac{b}{\nu}$$

$$W = w\frac{b}{\nu} = V_3\frac{b}{\nu} \quad .$$

The dimensionless pressure, temperature, time, and density, respectively, are defined by the equations:

$$P = P_1\frac{b^2}{\rho_0\nu^2} \quad ; \qquad \theta = \frac{T_1}{\Delta T_0} \quad ;$$

$$\hat{t} = \frac{t}{\Delta t_0} \quad ; \qquad \hat{\rho} = \frac{\rho_1}{\rho_0} \quad .$$

Rewriting Eqs. (2.13) in terms of these dimensionless variables, and rearranging the coefficients of various terms, leads to

Continuity :

$$\frac{b^2}{\nu(\Delta t_0)}\frac{\partial\hat{\rho}}{\partial\hat{t}} + \mathrm{div}(\vec{V}) = 0 \quad , \tag{2.14a}$$

Momentum :

$$\frac{b^2}{\nu(\Delta t_0)}\frac{\partial\vec{V}}{\partial\hat{t}} + (\vec{V}\cdot\overrightarrow{\mathrm{grad}})\vec{V} = \nabla^2\vec{V} - \overrightarrow{\mathrm{grad}}\,P + \frac{\Delta T_0\beta g b^3}{\nu^2}\theta\hat{i} \quad ,$$
$$+ \frac{1}{\nu}\left(\frac{\zeta + \frac{\mu}{3}}{\rho_0}\right)\mathrm{grad}\cdot\mathrm{div}\,\vec{V} \tag{2.14b}$$

Energy :

$$\frac{b^2}{\nu(\Delta t_0)}\frac{\partial\theta}{\partial\hat{t}} + (\vec{V}\cdot\overrightarrow{\mathrm{grad}})\theta = \frac{\alpha}{\nu}\nabla^2\theta + \frac{\nu^2}{\Delta T_0 C_p b^2}$$
$$\times\left[\frac{\mu}{\rho_0}\left(\frac{\partial V_i}{\partial X_k} + \frac{\partial V_k}{\partial X_i}\right)\frac{\partial V_i}{\partial X_k} + \left(\frac{\zeta - \frac{2\mu}{3}}{\rho_0}\right)\left(\frac{\partial V_\ell}{\partial X_\ell}\right)^2\right], \tag{2.14c}$$

where $\vec{V}$ now represents the dimensionless velocity vector and all the space derivatives are in terms of the dimensionless distances.

E. Dimensionless Numbers

Various groups of constants appear above in dimensionless groupings. Two of these are well-known in literature and have been given names: $\Delta T_0 \beta g b^3/\nu^2$ is called the Grashof number, usually denoted by Gr; ν/α is called the Prandtl number, usually denoted by Pr. The dimensionless combination $b^2/\nu(\Delta t_0)$ occurring in the first terms of Eqs. (2.14) will be denoted by $\hat{\text{Re}}$. (It is somewhat similar to the Reynolds number usually defined as bV/ν, but here does not have the usual significance attached to the Reynolds number.)

The other dimensionless groupings, appearing as coefficients of the last terms in Eqs. (2.14b) and (2.14c), will be left unnamed at the present in anticipation of the discussion in the next chapter, which shows that these terms can be dropped from Eqs. (2.14) so far as the behavior of air in buildings is concerned.

The three dimensionless groups Pr, Gr, and $\hat{\text{Re}}$ are discussed below in terms of their physical significance. These three numbers contain information about the essential features of the problem: two different physical situations having similar boundary conditions, and for which the numerical values of these dimensionless groups are the same, will have some solutions in terms of the dimensionless variables.

The Prandtl number ν characterizes the fluid properties rather than the particular flow. It is the ratio of the kinematic viscosity (momentum diffusivity), ν, to the thermal diffusivity α. In other words, it is a

measure of the relative strengths of diffusion of momentum (measured by kinematic viscosity $\nu = \mu/\beta$) and diffusion of thermal energy (measured with thermal diffusivity $\alpha = k/\rho C_p$). Fluids such as heavy oils have high Prandtl numbers (several hundreds); water has a strongly temperature-dependent Prandtl number that varies from 13.4 at 0°C to 1.9 at 93°C. Room air has a Prandtl number of about 0.7 and is relatively insensitive to temperature (0.713 at 275°K, 0.701 at 325°K). Liquid metals have very small Prandtl numbers, of the order of 10^{-3}.

The Grashof number gives a measure of the relative strengths of buoyant force and viscous force. The larger the value of the Grashof number, the higher the relative strength of the buoyant force (with respect to viscous forces). Gr is defined here as $\beta\Delta T\rho g b^3/\rho\nu^2$. The term $\beta\Delta T\rho g$, with dimensions of force/unit volume, is the buoyant force acting on a fluid element at temperature ΔT from the average. The denominator, $\rho\nu^2/b^3$, has the dimensions of force/unit volume, and is a measure of viscous force. The length b is a constant chosen to be characteristically representative of the dimension involved in the problem.

Due to the arbitrariness involved in the choice of the length scale b entering the definition, the Grashof number too has some arbitrariness. For example, for a room of aspect ratio 10, depending on whether one chooses b equal to the height of the room or the length of one side of the room, the Grashof number will differ by a factor of 10^3 (recall that b enters the definition of Grashof number raised to the third power).

This definition of Grashof number is not unique in another sense. In the literature, one sometimes finds Grashof defined in alternative ways

that produce a dimensionless group of variables, say, using heat flux instead of the temperature drop ΔT used in this definition (Ref. 21). Often, the Grashof number defined this way is denoted by Gr^* to distinguish it from the above definition of Grashof number:

$$Gr^* = \frac{\beta g \dot{q} b^4}{k\nu^2} \quad , \tag{2.15}$$

where $\dot{q}$ is the heat flux and k is the thermal conductivity of the fluid.

For future reference, we introduce here another related dimensionless number called the Rayleigh number, usually denoted by Ra. Ra is defined by

$$Ra = Gr \cdot Pr \quad .$$

The Rayleigh number is a measure of the relative strengths of convective to conductive processes. For Rayleigh numbers below 10^4, the boundary layer approximation for the flow becomes invalid. A Rayleigh number of larger than $\sim 10^4$ is indicative of the onset of convection (Ref. 22).

Experimental results indicate that for a hot isothermal flat vertical plate in a bath of cool fluid, the flow developing along the plate becomes turbulent for values of $Ra \gtrsim 10^{10}$ (Ref. 23). In situations (such as cavities) where the flow is more restricted, one can expect the transition to turbulent flow to occur at a somewhat larger value of Ra.

The third dimensionless group denoted here is $\hat{Re} = b^2/\nu(\Delta t_0)$. This is a dimensionless inverse of the time step (Δt_0) introduced in the earlier section. This time step will be used in the iterative solution of the flow fields and the temperature fields, and this is not a characteristic of the fluid nor of the flow under study. It should be noted here that

for $b = 3m$, and $\nu = 1.54 \times 10^{-5} m^2 sec^{-1}$ (for room air), a value of $\hat{Re} = 10^5$ implies a Δt_0 of 5.7 sec, and a perfect inverse relation holds between $\hat{Re}$ and (Δt_0).

CHAPTER 3

SIMPLIFICATION OF EQUATIONS AND THE NUMERICAL SCHEME

3.1 Introduction

In Chapter 2, the equations governing fluid flow were developed and briefly examined in order to ascertain the physical meaning of each of the terms occurring in them. A few assumptions were made to simplify the expressions without significantly affecting their generality. These equations [Eq. (2.14) of Chapter 2], however, still contain many terms that become insignificantly small, or that have a negligible influence on the solution for the problem of interest to us. These terms must be identified and dropped from the equations. Several additional assumptions can be justified which further simplify the equations at the expense of introducing errors of only a few percent. After dropping the insignificant terms and making the simplifying assumptions, the equations still remain quite formidable. However, a numerical scheme, or a solution procedure, can be devised in order to solve the equations under a specified set of boundary conditions.

This chapter describes the simplification of the full Navier-Stokes equations and outlines the numerical scheme used for obtaining the solutions to these simplified equations.

3.2 Identifying Insignificant Terms in the Governing Equations

The second term on the right-hand side of the energy equation, (2.14c), represents dissipation of mechanical (kinetic) energy of the

fluid through viscous effects and appearance of this energy as heat. A good measure of the importance of this term in a given problem is given by the ratio of the changes of mechanical to thermal energy, i.e., by the quantity:

$$\frac{\frac{1}{2}\rho\left(V_{max}^2 - V_{min}^2\right)}{\rho C_p \Delta T}$$

If this ratio is close to one (or larger), the changes involved in kinetic energy are substantial enough to demand the inclusion of the viscous heating term in the energy equation. Such is the case in problems involving supersonic projectiles moving through a fluid, shock waves, atmospheric re-entry of spacecraft, etc. For flow of buoyant air in a room, the velocities encountered are no more than about 20 cm/sec, while ΔT is of the order of 10°C. This leads to a value of ~0.002 for the above ratio. This means that the pool of kinetic energy available for possible conversion into thermal energy is insignificant compared to the thermal energy flows arising due to the boundary conditions on temperature, and this term in the energy equation can be neglected in the problem under consideration.

Next consider changes in the density of the fluid. These changes can occur due to: (1) pressure changes, and (2) thermal expansion. In the former case, if the flow is steady and laminar, the fluid flows along streamlines* defined by

*For steady flow, fluid particles flow along streamlines. For unsteady flow, the streamlines can still be defined by taking space and time averages; but paths of individual fluid particles will not coincide with the "averaged" streamlines.

$$\frac{dx}{u} = \frac{dy}{v} = \frac{dz}{w} \quad ,$$

where u, v, and w are components of local fluid velocity along x, y, and z directions, respectively. We can apply Bernoulli's principle since the flow is steady ($d\vec{V}/dt = 0$). Bernoulli's principle, which is a special case of conservation of mechanical energy applied to an element of fluid in a steady laminar flow, can be used to get an order of magnitude estimate of the pressure change involved in the fluid flow. It states that, at any point "a" along a streamline, the quantity

$$\Phi_a + \frac{V_a^2}{2} + \int_0^a \frac{dp}{\rho}$$

is a constant. V_a is the local fluid velocity at point a. The integral $\int_0^a dp/\rho$ is evaluated from some reference point 0, along the streamline, to the observation point a, and Φ_a is the potential (in this case, gravitational potential) at a with respect to 0 due to an external conservative force field acting on the fluid. From this, one can estimate the pressure drop involved in the buoyant flow to be:

$$\delta p = \tfrac{1}{2}\rho V^2 + \rho\Phi_a \cong \rho V^2 \quad . \tag{3.1}$$

(Since the flow is arising from gravitational [buoyant] forces, $\frac{1}{2}\rho V^2$ can be at most only as large as $\rho\Phi_a$.) Using the relation for velocity of sound, C_s:

$$C_s^2 = \frac{\partial p}{\partial \rho} \quad , \quad \therefore \quad \delta p = C_s^2\, \delta\rho, \tag{3.2}$$

and combining (3.1) and (3.2), one obtains:

$$\frac{\partial\rho}{\rho} \cong \frac{V^2}{C_s^2} \quad .$$

Thus one can safely neglect terms involving derivatives of density $\delta\rho/\rho << 1$ so long as $V^2/C_s^2 << 1$. C_s for air at normal temperature and pressure (NTP) is 300 m/sec, while V_{max} for the regime of interest is $\lesssim 0.2$ m/sec. Thus the approximation is well-justified.

For non-steady (i.e., oscillating and laminar or turbulent) flow, the momentum equation (2.2) can be used to estimate $(\delta\rho/\rho)$. Applying this equation one obtains

$$\frac{V}{\tau} \sim \frac{\delta p}{L\rho} \quad ,$$

where τ is the characteristic time-scale of motion and L is the characteristic dimension for flow to change significantly. Therefore,

$$\delta p \sim \frac{LV\rho}{\tau} \quad .$$

Again, using the relation for velocity of sound (3.2), this leads to

$$\delta p \sim \frac{LV\rho}{\tau C_s^2} \quad . \tag{3.3}$$

If incompressibility is assumed, then in the continuity equation (2.1):

$$\frac{1}{\rho}\frac{d}{dt} << \vec{\nabla}\cdot\vec{V} \quad ;$$

i.e., if

$$\frac{\delta\rho}{\tau} << \frac{\rho V}{L} \qquad \text{or} \qquad \frac{\delta\rho}{\rho} << \frac{\tau V}{L} \quad .$$

Substituting for $\delta\rho$ from Eq. (3.3) above, this condition becomes

$$\frac{LV}{\tau C_s^2} \ll \frac{\tau V}{L}$$

i.e.,

$$\left(\frac{L}{\tau}\right)^2 \ll C_s^2 \quad ,$$

where C_s = 300 m/sec, $L \cong 3$ m, and $\tau \gtrsim 1$ sec. This condition is satisfied by either turbulent or oscillating laminar air flow encountered inside buildings. Thus the assumption of incompressibility is well-justified for this regime also.*

Thus, subsequent calculations can safely neglect density changes due to change in velocity of flow or due to changes in pressure in the enclosure. The above analysis shows these changes to be totally negligible in magnitude (less than 1 part in 10^4).

The second process which produces density changes is the presence of differences in air temperature. In contrast to the density changes arising from pressure changes, it is clear that not only are these effects larger in magnitude (about 5 parts in 100), but also they are decisively important to the air flow. It is these density changes that give rise to the buoyancy forces that drive the flow. Ignoring these density changes would reduce the problem to one of pure conduction. However, an approximation allowing one to neglect the terms involving derivatives of density from the equations of flow [Eqs. (2.14) of Chapter 2] is obviously very attractive. Such an approximation would not only eliminate one more variable, but would substantially simplify the form of the

---

*Pressure fluctuations in a turbulent flow do not affect the mean density.

equations to be solved.

Precisely such an approximation was suggested more than 50 years ago by Boussinesq. He suggested that one can simplify the problem without sacrificing accuracy substantially if one keeps the buoyancy term in the momentum equations (the term involving δ_{i3} in the momentum equation), but ignores all the other terms involving derivatives of density. With this approximation the effects of thermal expansion appear only as a body force term in the momentum equations. Daly and Pracht (Ref. 24) have solved buoyancy problems on a computer both with and without the Boussinesq approximation. They conclude that so long as the value of $\beta\Delta T$ remains less than 0.3 (i.e., the fluid expands less than 30% during the flow), the error introduced due to the Boussinesq approximation is less than 5% (in our calculations, $\beta\Delta T_{max} \cong 0.05$).

Another simplifying approximation will be made when solving these equations. We shall consider the physical properties of air to be constant over the temperature range of interest. The physical properties of air enter the calculations through two variables: the Prandtl number and the Grashof number. Over the range of 0-50°C, the Prandtl number for air decreases by 2%, and the Grashof number, for a given ΔT and L, decreases by a factor of 0.47 (Ref. 25). In the calculational procedure used here, it is possible to take into account these changes by calculating the local values of the Prandtl and Grashof numbers every time they appear in the equation. In fact, for a problem involving buoyancy-driven flow in water, one would probably find it necessary to do this. But for air flows inside buildings, the error introduced into the calculations by ignoring the variation in physical properties of air is small enough,

if one makes sure that when deducing the actual (dimensional) heat fluxes from surfaces, etc., one uses the proper values of physical properties of air.

With these two approximations, the equations to be solved reduce to:

Continuity:

$$\text{div}(\vec{V}) = 0 \quad , \tag{3.4a}$$

Momentum:

$$\hat{\text{Re}} \frac{d\vec{V}}{dt} + (\vec{V} \cdot \vec{\nabla})\vec{V} = \nabla^2 V - \text{grad } p + \text{Gr}\theta \, \delta_i^3 \quad , \tag{3.4b}$$

Energy:

$$\hat{\text{Re}} \frac{\partial \theta}{\partial t} + (\vec{V} \cdot \text{grad})\theta = \frac{1}{\text{Pr}} \nabla^2 \theta \quad . \tag{3.4c}$$

where we have written t for the variable $\hat{t}$ of Eqs. (2.14). Equations (3.4), together with the appropriate boundary conditions, define the problem completely. Since the temperature boundary conditions inside rooms change only slowly,* it is acceptable to seek steady-state, time-independent solutions to these equations. This is not to say that we neglect turbulent fluctuating flow; instead, we mean that transient phenomena such as the details of how the flow starts, etc., are not of prime importance to the particular problem of building physics that is being addressed here.

Equations (3.4) comprise a set of five coupled partial differential

*The flow is set up in a few minutes, while the boundary conditions change typically over a period of hours.

equations [Eq. (3.4b), expressed in vector notation, is really three equations]. The equations are of second order and are nonlinear, i.e., an arithmetic multiple of the solution fields will not, in general, satisfy the equations; thus, the principle of superposition is not applicable.

3.3 Brief Review of the Relevant Sections from the Theory of Partial Differential Equations

Second-order partial differential equations in one independent variable are classified into parabolic, elliptic, or hyperbolic in much the same way as one classifies a second-order algebraic equation in two variables. In general, one can write a quasi-linear second-order partial differential equation as

$$\sum_{m,n=1}^{N} a_{mn}(x_i) \frac{\partial^2 u}{\partial x_m \partial x_n} + F\left(x_i, u, \frac{\partial u}{\partial x_j}\right) = 0 \quad . \qquad (3.5)$$

(The equation is called quasi-linear, meaning linear with respect to the highest partial derivative.) By a suitable orthogonal transformation, the symmetric matrix formed by elements $[a_{mn}(x_i)]$ can be diagonalized. The same transformation on the independent variables will yield new variables y_i in terms of which, in Eq. (3.2), all mixed second-order derivatives disappear (i.e., terms of type

$$\left.\frac{\partial^2 u}{\partial y_i \partial y_j}\right|_{i \neq j}$$

are eliminated from the equation). This fact is used in the classification of equations of the type (3.5) (Ref. 26). Let the new variables be

denoted by x_{io}, $i = 1,\ldots,N$. Then,

(1) Equation (3.5) is of the parabolic type at the point $x = x_{io}$ $(i = 1,2,\ldots,N)$ if at least one of the coefficients $a_k(x_{io})$ is zero.

(2) Equation (3.5) is of the ultrahyperbolic type at the point $x_i = x_{io}$ $(i = 1,2,\ldots,N)$ if all the coefficients $a_k(x_{io})$ $(k = 1,2,\ldots,N)$ are non-zero but do not have the same sign. In particular, Eq. (3.5) is of the hyperbolic type if only one coefficient among the $a_k(x_{io})$ $(k = 1,2,\ldots,N)$ has a sign different from all others.

(3) Equation (3.5) is of the elliptic type at the point $x_i = x_{io}$ $(i = 1,2,\ldots,N)$ if all the coefficients $a_k(x_{io})$ $(k = 1,2,\ldots,N)$ are non-zero and have the same sign.

Familiar examples of elliptic, hyperbolic, and parabolic types of equations are, respectively:

Laplace's equation:
$$\frac{\partial^2 u}{\partial x^2} + \frac{\partial^2 u}{\partial y^2} = 0 \quad ; \tag{3.6}$$

the wave equation:
$$\frac{\partial^2 u}{\partial x^2} - \frac{\partial^2 u}{\partial y^2} = 0 \quad ; \tag{3.7}$$

the diffusion equation:
$$\frac{\partial^2 u}{\partial x^2} - \frac{\partial u}{\partial t} = 0 \quad . \tag{3.8}$$

The existence of a solution of any of the three types of equations is closely connected with the specification of the boundary conditions. Recall that a single equation in the independent variables, $S(x_1,x_2,\ldots,x_N) = 0$, defines a hypersurface in the space of these variables. Recall also

that the boundary conditions specified on such a hypersurface for second order partial differential equations are classified into three types:

(a) Cauchy boundary condition is specified when the values of the unknown function $U(x_1, x_2, \ldots, x_N)$ and of its partial derivatives along a direction normal to a hypersurface are prescribed.

(b) The Dirichlet condition consists in prescribing only the values of the unknown function on a hypersurface.

(c) For the Neumann condition, only the values of the derivatives of a function along the normal to a hypersurface are described.

The literature (see e.g., Ref. 26) contains the following rule of thumb to indicate general correlation between the types of the equations and the types of boundary conditions that may lead to a stable solution of the differential equation:

(a) Elliptic equations: Dirichlet or Neumann conditions on a closed hypersurface.

(b) Parabolic equations: Dirichlet or Neumann conditions on an open hypersurface. A stable solution exists on one side of the hypersurface only.

(c) Hyperbolic equations: Cauchy conditions on an open hypersurface. If the hypersurface is finite, the Cauchy conditions must be supplemented by Dirichlet or Neumann conditions on another hypersurface.

An examination of Eqs. (3.4) shows that, in general, the equations are of the elliptic type and we will need a Dirichlet or Neumann boundary condition on a closed surface. In some particular application of these equations, such as, for example, fluid flow in one direction without recirculation (e.g., air flow in a Trombe wall channel), the equations can be put in parabolic form and they then require different boundary conditions. See Refs. 14 and 27 for such an application. For flow in a room, there is recirculation in all three directions and the equations are truly elliptic.

For parabolic flows, it is possible to solve the flow equations numerically by using a "marching procedure"; it is so called since one begins the evaluation of flow fields from the upstream position where Dirichlet or Neumann conditions are specified on an open hypersurface. The solution procedure then involves "marching" in the downstream direction evaluating the new flow fields at each new grid plane using the values of the flow fields at the upstream grid planes. Since the flow has no recirculation in the direction of marching, one can evaluate the flow fields at an upstream plane without having to worry about the flow behavior at the downstream positions. Notice here that recirculation in directions orthogonal to the direction of main flow still would allow application of the marching procedure, provided one accounted for recirculation within each grid plane as one marched along the flow in the downstream direction. This important advance is documented and described in Ref. 27. This simplification is not obtained for elliptic flows, where there are no "downstream" and "upstream" locations for the flow as a whole (except locally, where for a definite local velocity direction

there still can be defined locally upstream and locally downstream points, in the immediate neighborhood of the point of interest).

Thus the numerical procedure for elliptic flows has to proceed, generally, using iterative evaluation of the flow fields at various grid points spaced throughout the volume under investigation. The coupled and nonlinear character of the equations, though intimidating for an analytic approach to the solutions, produces no essential complications for an iterative procedure. So long as one can ensure that at each iteraction, the fields are being updated towards the correct solution, one can generally be confident that convergence can be obtained.

The objective of the numerical solution procedure to be used here is to determine the velocity field $\vec{V}$ and temperature field θ which satisfy the equations (3.4) and the imposed boundary conditions. To determine these fields, the space is divided into finite and discrete cells, each centered around a grid point. The fields are evaluated at each of the grid points and the value of the variable at each grid point will be the value of that variable averaged over the cell surrounding the point. The choice of the grid scheme is influenced by the geometry of the problem, the nature of the expected flow, and the choice of the discretization scheme.

3.4 The Solution Procedures

To approximate the field by a finite number of grid points implies that the differential equations (3.4) must be converted into difference equations. These equations are then solved, usually by iteration, to obtain the various field variables at the grid points.

There is an obvious difficulty in the solution of Eqs. (3.4); given the velocity field, one can think of solution procedures for obtaining the temperature field (by, say, iteration) under the given temperature boundary conditions, by solving Eq. (3.4c). Also, if the pressure field P is known, one can solve Eq. (3.4b) for the velocity field, given the boundary conditions. The nonlinearity of the velocity equation (3.4b) and the linkage between (3.4c) and (3.4b) [introduced through buoyant body-force term $Gr \cdot \theta \cdot \delta_i^3$ in (3.4b)] can be handled by iteration. However, the calculation of the pressure field is indeterminate; pressure builds up where inflow exceeds the outflow, and drops down wherever outflow exceeds inflow. This pressure field, acting on the momentum equation (3.4b) (via the $\vec{\nabla}P$ term) enforces the continuity equation. But as the equations stand, there is no way of obtaining this pressure field.

For two-dimensional elliptic problems, the popular approach is to cast the equations (3.4) in terms of a stream function and vorticity field. The pressure is eliminated from the momentum equations by differentiating the u equation by y and the v equation by x and subtracting one from the other. The vorticity ζ is defined as

$$\zeta = \frac{\partial u}{\partial y} - \frac{\partial v}{\partial x} \quad .$$

One thus obtains the governing equation for vorticity. The stream function ψ is defined by

$$\frac{\partial \psi}{\partial y} = u \quad , \qquad \frac{\partial \psi}{\partial x} = -v \quad .$$

The stream function and vorticity are therefore related by

$$\nabla^2\psi = \zeta \quad .$$

The continuity equation can be incorporated into the transport equation for ζ by using a vector identity.

In extending this approach to three dimensions, one has to work with a vorticity vector in place of the scalar vorticity used in two-dimensional problems (for example, see Ref. 28). The concept of stream function becomes meaningless. In its place we use a velocity potential vector. Thus we now deal with six components in all, whose physical meaning is not immediately obvious. This approach is thus more complicated than that using the primitive variables $\vec{V}$ and P for three dimensions.

The approaches using $\vec{V}$ and P can be extended to two or three dimensional solutions with little modification and the schemes intended for two dimensions can easily be extended to three-dimensional problems. The essential differences in the various schemes using $\vec{V}$ and P as the variables to be solved lies in the way the finite difference equations are set up and the choice of the grid system.

Several authors have constructed schemes for handling the $(\vec{V},P)$ variables; among these are the pioneering work of the Los Alamos group (Ref. 29) and the papers by Chorin (Ref. 30), Piacsek and Williams (Ref. 31), and Deardorff (Ref. 32) and Thommen (Ref. 33). These methods, except that of Deardorff, have been applied extensively to laminar flow. Deardorff has calculated the turbulent velocity fluctuations by actually calculating the unsteady laminar motion of fluid elements. Application of these methods with turbulent models in three-dimensional situations

is very rare (Ref. 34). Our calculational approach follows the formulation of Patankar and Spalding in their recent works (Ref. 35).

The numerical solution technique attempts to find the steady-state solution by starting from initially specified values of the field variables $(\vec{V},P,\theta)$ and iteratively calculating the values of the flow fields at successive incremental values of time, by using the time-dependent governing equations of the kind (3.4). This is continued until a converged solution is reached. (By converged solution, we mean that the fractional change in the flow fields from one iteration to the next is less than some prescribed number. In the literature, this number ranges anywhere from 10^{-3} to 10^{-8} (Ref. 36).)

The pressure is calculated using the continuity equation; the grid points where $\text{div}\cdot\vec{V}$ is positive being assigned lower values of P, and the grid points where $\text{div}\cdot\vec{V}$ is negative being assigned higher values of P for the next iteration. The magnitude of this change in the value of P is determined from the (local) magnitude and sign of $\text{div}\cdot\vec{V}$ and from the relative strength of the coefficient with which (grad p) enters the equation for calculating the (local) values of velocity components (Ref. 37).

It should be noted here that the procedure will find steady-state solutions to the Eqs. (3.4). If under the boundary conditions and other particularities of the situation the flow should in fact exhibit an oscillatory character (by this is meant steady, laminar, oscillatory flow before transition to full turbulence), the calculational procedure has no definite way of determining this and will try to converge to a steady-state solution. For solution of turbulent flows, equations of a turbulence

model can be added to Eqs. (3.4) and be incorporated in the calculational sequence. Of course, in the absence of such equations, the calculational sequence will try to converge to a laminar solution for a situation where the real flow will actually be turbulent. The appropriateness of a particular choice of solution procedure or modeling equations must, of course, be finally judged by comparison with experiment.

The second point to be noted is that "convergence" as used above is with reference to the development of the flow fields with iterations. Another meaning of the word "convergence" applied to a numerical solution procedure is that in the limit as the size of discretized steps (ΔX, ΔY, ΔZ and Δt) used in the numerical scheme goes to zero, the discretized equations should converge to the original differential equations. (Trivial as this requirement may seem, it is possible to make mistakes in the discretization and solve the wrong differential equation as a result!) The differencing scheme employed here (below) satisfies this requirement of convergence in the limit of $\Delta X, \Delta Y, \Delta Z, \Delta t \to 0$.

We begin by rewriting Eqs. (3.4) in a more convenient form; note that for any field variables ϕ, we can write

$$(\vec{V} \cdot \text{grad})\phi = \text{div}(\vec{V}\phi) - \phi \text{div} \cdot \vec{V} = \text{div}(\vec{V}\phi)$$

(since $\text{div} \cdot \vec{V} = 0$). ϕ can take values of the velocity components in Eq. (3.4b), or θ in Eq. (3.4c). Thus, Eqs. (3.4) can be rewritten as:

Continuity:

$$\text{div}(\vec{V}) = 0 \tag{3.11a}$$

Momentum:

$$\hat{\text{Re}} \frac{\partial \vec{V}_i}{\partial t} + \text{div}(\vec{V} \cdot \vec{V}_i) = \nabla^2 \vec{V} - \text{grad } p + \text{Gr}\theta\delta_3^i \tag{3.11b}$$

Energy:

$$\hat{Re}\,\frac{\partial\theta}{\partial t} + \mathrm{div}(\vec{V}\theta) = \frac{1}{Pr}\,\nabla^2\theta \quad . \tag{3.11c}$$

The solution procedure for Eqs. (3.11) will be described below in three sections, each relating to (1) the difference equations, (2) the choice of grids, and (3) the iterative procedure.

A. The Difference Equations

The space of interest is assumed to be a rectangular parallelpiped. We construct a rectangular grid that fills this entire space of interest. The axes of the grid are parallel to the edges of the (rectangular parallel-piped) space, which are also aligned with the coordinate axes. Figure 2 shows a representative node P of this grid with its neighbors.

The node P is surrounded by the neighboring grid nodes N (north) and S (south) along the ±Z axis; E (east) and W (west) along the ±Y axis; and U (up) and D (down) along the ±X axis, at distances PN, PS, PE, PW, PU, and PD, respectively (these distances are not necessarily equal). The control volume surrounding the grid node P is formed by planes that perpendicularly bisect the line segments PN, PS, etc. at points n, s, e, w, u, and d, respectively. The finite difference equations are obtained by integrating the equations (3.11) over the control volume.

The time is discretized into time steps of size Δt. From the known values of the variables at time t, we want to find their values at time $t+\Delta t$. There are, in general, two approaches for achieving this. One can either update the variable at each grid node individually, using the old values of the variable at all other grid nodes or one can update all

the grid nodes simultaneously. The former approach is called the "explicit" method and the latter the "implicit" method.* Explicit methods are simpler to formulate and solve, but have an upper limit on the largest time step that is acceptable without leading to divergence. Implicit methods, on the other hand, are somewhat more complicated to formulate and generally require matrix inversion to calculate the variables at the new time $(t+\Delta t)$, but have no such limitation on the size of the maximum allowable time step. Since the steady state situations are of interest here, it is desirable to use quite large values of Δt; therefore, the implicit method of solution is selected.

Equation (3.11c) can be written in the following form

$$\hat{Re}\,\frac{d\theta}{dt} = -\vec{\nabla}\cdot(\theta\vec{V}) + \frac{1}{Pr}\,\vec{\nabla}\cdot(\vec{\nabla}\cdot\theta) \quad . \tag{3.12}$$

(Note that the equations are all in dimensionless variables from now on.) Integrating over the control volume, the left-hand side of (3.12) yields

$$\frac{\hat{Re}(\theta_p - \theta_p^0)(\Delta X\,\Delta Y\,\Delta Z)}{\Delta t}$$

where the superscript "0" denotes values at time t, and its absence denotes values at times $t+\Delta t$. $(\Delta X \Delta Y \Delta Z)$ is the volume of the control element and Δt is the time step. The terms on the right-hand side of Eq. (3.12) give rise to surface integrals via Gauss's theorem. For

*To be more precise, the explicit method uses the values of variables at time t for computing spatial derivatives used in the equation for evaluating the variable at time $t+\Delta t$. The implicit method uses the (unknown) values of variables at time level $t+\Delta t$ for calculating the spatial derivatives in the equation for evaluating the variable at time $t+\Delta t$.

reasons described below, we will consider them together.

Consider the face marked "area FE" of the control volume between points P and E in Fig. 2. To evaluate the contribution of this face to the surface integral, one must make an assumption about the way θ varies between P and E; make an educated guess about the average value of θ on this face midway between P and E. If one assumes that θ varies linearly between points P and E, the contribution C_e of this face to the surface integral arising from integrating the right-hand side of (3.12) is

$$C_e = -V_e FE \frac{\theta_P + \theta_E}{2} + \frac{1}{Pr} FE \frac{\theta_E - \theta_P}{PE} , \qquad (3.13)$$

where V_e is the V-component of the velocity evaluated at point e.* As shown below, this formulation must be modified under certain circumstances depending on the magnitude and direction of V_e.

Similar contributions from the other five faces of the control volume will appear in the full equation. When all the terms are added together, the general form of the equation will be:

$$A_P\theta_P = A_E\theta_E + A_W\theta_W + A_N\theta_N + A_S\theta_S + A_U\theta_U + A_D\theta_D + B \qquad (3.14)$$

where the coefficients A are given by, for example,

*Other assumptions of variations of variables lead to different formulations of the difference equations. See, for example, Raithby and Torrence (Ref. 38).

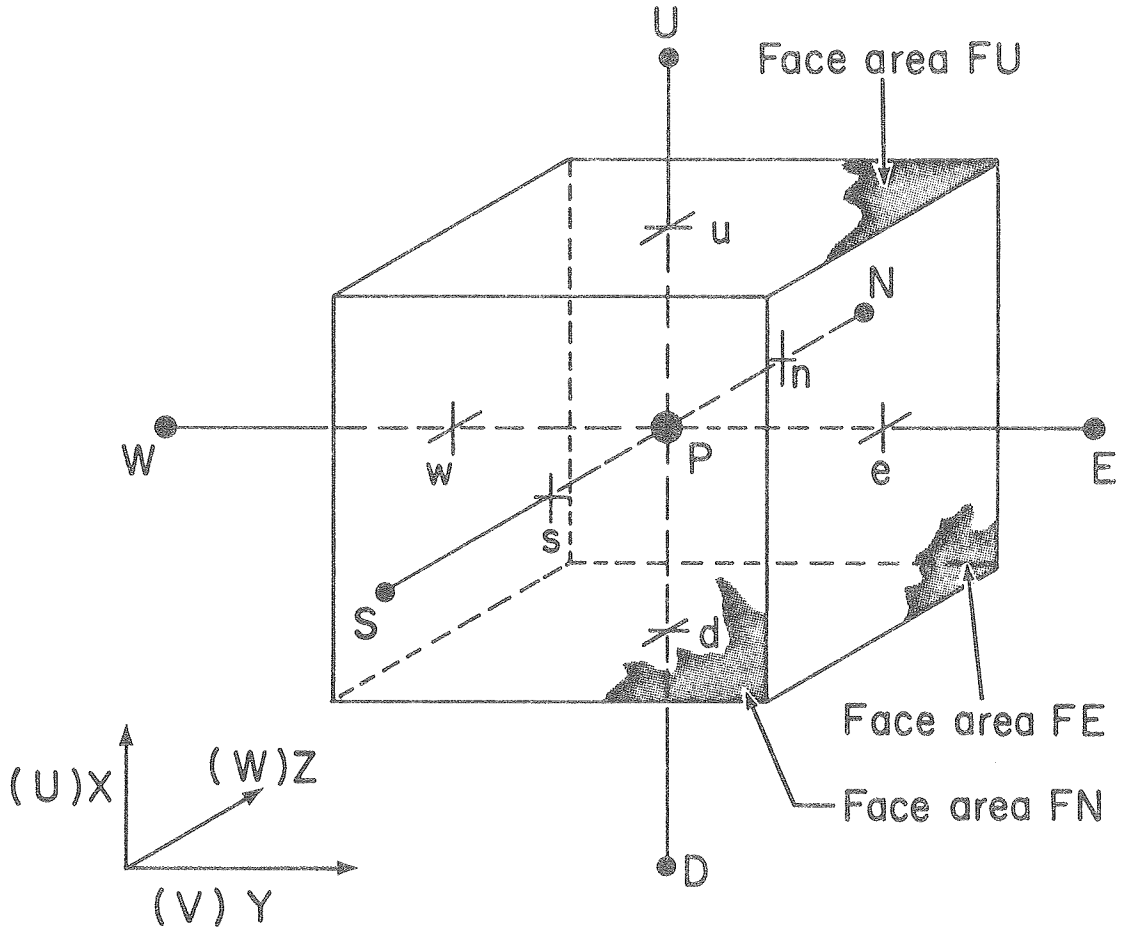
U
Face area FU
u
N
n
W
w
P
e
E
s
S
d
Face area FE
Face area FN
D
(U)X
(W)Z
(V) Y
XBL7910-13111

Fig. 2

$$A_P = FE\left(\frac{1}{Pr \cdot PE} + \frac{1}{Pr \cdot PW} + \frac{V_e}{2} + \frac{V_w}{2}\right)$$

$$+ FN\left(\frac{1}{Pr \cdot PN} + \frac{1}{Pr \cdot PS} + \frac{W_n}{2} + \frac{W_s}{2}\right)$$

$$+ FU\left(\frac{1}{Pr \cdot PU} + \frac{1}{Pr \cdot PD} + \frac{U_u}{2} - \frac{U_d}{2}\right) + \frac{\Delta X\, \Delta Y\, \Delta Z}{\Delta t} \cdot \hat{Re}$$

$$A_E = FE\left(\frac{1}{Pr \cdot PE} - \frac{V_e}{2}\right)$$

$$A_W = FE\left(\frac{1}{Pr \cdot PW} + \frac{V_w}{2}\right)$$

$$\vdots$$

$$B = \frac{\theta_P^0\, \Delta X\, \Delta Y\, \Delta Z}{\Delta t}$$

and where all the θ values are at time $t + \Delta t$; B contains the value of θ at time t. In solving Eq. (3.14) for θ_P, the temperature at node P is a function of the temperature at all surrounding grid nodes. Specifically, the dependence of θ_P on, for example, θ_E can be determined by rearranging (3.13)

$$\frac{\hat{Re}(\Delta X \Delta Y \Delta Z)}{\Delta t}\ \theta_P = FE\left(\frac{1}{Pr \cdot PE} - \frac{V_e}{2}\right)\theta_E + \text{other terms} \quad . \tag{3.15}$$

The magnitude and sign of $(V_e/2)$ with respect to $(1/Pr \cdot PE)$ can make the coefficient of θ_E in the above equation positive or negative. A large positive V will make this coefficient negative. Similarly, a large negative V will make the coefficient of θ_W negative, and so on.

Physically, it is implausible that an increase of temperature at E should lead to a decrease in temperature at P. Thus negative coefficients are physically implausible. Of course, what is happening is that at large positive values of V, θ_E will be downstream of θ_P and should have practically no effect (and certainly not a negative effect) on θ_P. To see more clearly why this unacceptable result was obtained, one must go back to the assumptions made in deriving Eq. (3.13). It was assumed that there was a linear variation of values of θ between nodes P and E. But if the component of velocity is sufficiently large, the convection effects will completely dominate the diffusion effects in the x-direction. Then a better approximation to the value of θ at point e will be θ_P [instead of $(\theta_P + \theta_E)/2$]. Also, since the value of θ_P is being convected towards E much more strongly than the diffusion of θ_E towards P, the diffusion flux across the face FE in Fig. 2 will be negligible. Thus we must modify the coefficients A in Eq. (3.14), taking into account the local magnitude and sign of the velocity vector, such that these coefficients are never negative. This is precisely what the hybrid formulation achieves, as shown below.

The hybrid formulation (so called because it is a hybrid of the "central" and "upstream" difference schemes) considers the direction and magnitude of the local fluid flow and determines how the difference equation is to be formulated. If the fluid velocity is sufficiently high so that the contribution from the downstream node is going to be negative and the contribution from the upstream node is going to be large [as formulated in Eq. (3.13)], then the hybrid formulation modifies the difference equation for that grid node and for that time step from a

"central difference" formulation [as incorporated in (3.13)] to an "upstream difference" formulation. In the upstream difference formulation, the variable at the grid node upstream of node P is allowed to completely dominate the equation for the new value of θ_P, while the variable at a node downstream of P does not appear in the equation at all. In physical terms, the downstream convection of the value of the variable has now begun to dominate the diffusion of the value of that variable against the direction of the flow.

For this purpose, one must examine the coefficients such as that on the right-hand side of (3.15)

(1) If $\frac{1}{Pr \cdot PE} > \left|\frac{V_e}{2}\right|$, i.e., if $|V_e \cdot PE \cdot Pr| < 2$, then the coefficient is positive and the expression C_e is left as it appears in (3.13).

(2) If $V_e \cdot PE \cdot Pr \geq 2$, then V_e is sufficiently large to dominate the diffusion effects, and $C_e = -V_e \cdot Fe \cdot \theta_P$.

(3) If $V_e \cdot PE \cdot Pr \leq -2$, then again V_e is so large that diffusion effects are small; however, in this case, the direction of the convection is opposite to that in case (2) above. Then, $C_e = -V_e \cdot FE \cdot \theta_E$.

These values of C_e in turn lead to the following choices for the coefficient A_E of θ_E in Eq. (3.14):

$$A_E = \begin{cases} (1/Pr \cdot Pe - V_e/2)FE & \text{for } |V_e \cdot PE \cdot Pr| < 2 \\ 0 & \text{for } V_e \cdot PE \cdot Pr \geq 2 \\ -V_e \cdot FE & \text{for } V_e \cdot PE \cdot Pr \leq -2 \end{cases}$$

Such an evaluation is made for each of the coefficietns A in Eq. (3.14).

For a more detailed justification and explanation of this scheme, see Appendix A, and Refs. 19 and 39.

Other schemes exist for ensuring that the difference scheme will yield physically significant results by always satisfying part (1) of the above scheme, i.e., keeping $|V_e \cdot PE \cdot Pr| < 2$. Taking small enough grids will reduce PE and satisfy the inequality; using an artificially small Pr (the method of artificial viscosity) will also suffice. These schemes lead to compromises too; these might be in terms of the need for large computer times and storage requirements, or the complications associated with estimating the amount of artificial viscosity needed and its presence in those regions where it is not needed in order to obtain acceptable solutions.

B. The Grid Construction

The choice of the grid scheme (in which we formulate the equations) is influenced by the considerations that the flow properties should be conserved across the face of the control volume. One must set up the equations in such a way that what is calculated to be leaving one control volume through a particular face is identical to what is calculated to be entering the neighboring control volume sharing that particular face. Experience has shown that though conservation need not be an essential property of a numerical solution scheme, conservative systems do generally give more accurate results (Ref. 40). Torrance et al (Ref. 41) have shown how, for the driven cavity problem, the use of conservative equations of only first order accuracy is more accurate than the use of non-conservative

equations of second order accuracy. The conservative requirement is not completely trivial. Consider, for example, the two neighboring control volumes centered around nodes A and B with a common face denoted by *ab*. If one assumes that the fluid leaving the control volume surrounding A (here denoted by [A] for brevity) leaves with temperature, viscous diffusivity, and velocity calculated at node A, and crosses the face *ab* entering in [B] with temperature, viscous diffusivity, and velocity calculated at node B, inconsistencies may arise. To avoid this, one must therefore calculate these properties at the common face *ab* somehow.

Further, two peculiar problems turn up even if one makes the calculation of velocities at the common face by averaging the velocities of the neighboring grid nodes of each face. Consider the one-dimensional flow field depicted in Fig. 3. This flow field is conservative, as defined above, despite its being unacceptable as a realistic flow field. (For simplicity, we have shown only a one-dimensional situation, but one can easily see the problem getting more complicated in two or three dimensions.) A, B, C, D, and E are grid nodes centered at the control volumes [A], [B], [C], [D], and [E], respectively, with common faces *ab* *bc*, *cd*, *de*, etc. A hypothetical velocity distribution is shown in Fig. 3 with velocity at each grid node being written near it.

The velocity of fluid at each face is 175 units (average of -50 and 400) and so it appears that the above distribution of velocities satisfies the continuity equation for each control volume, and hence for the entire space, exactly. In this example, the principle of calculating velocity at the faces of the control volumes has been strictly followed.

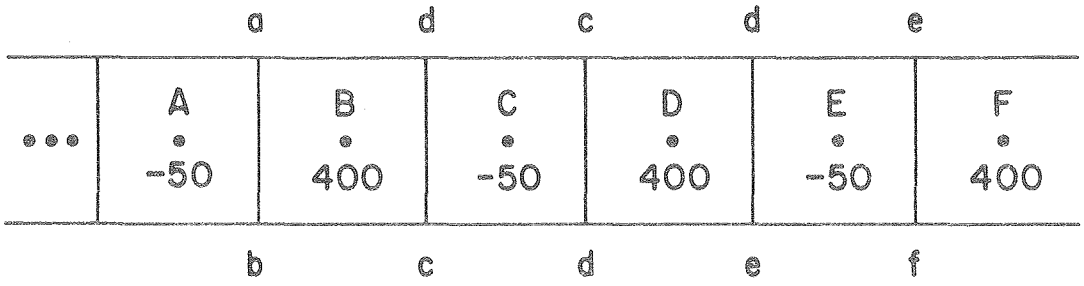

A HYPOTHETICAL ONE-DIMENSIONAL VELOCITY DISTRIBUTION, WHERE THE VELOCITIES ARE EVALUATED AT THE CENTER OF THE CONTROL VOLUME. THIS VELOCITY FIELD SATISFIES THE DISCRETIZED CONTINUITY EQUATION MENTIONED IN THE TEXT.

XBL7911-13113

Fig. 3.

Now consider Fig. 4. This figure shows a hypothetical pressure distribution that may develop in the process of solving the equations. Consider the effect of this pressure distribution on a control volume, say [C].

A pressure difference of 300 units acts on the face *bc* of [C] and a pressure difference of 300 units acts on the face *cd* of [C] in the opposite direction. Thus the net force felt by [C] due to this pressure distribution is zero; this is true of every control volume, and hence of the entire space of interest. In other words, a pressure distribution like that shown above, though unacceptable, is indistinguishable from zero pressure everywhere for our difference scheme.

From these considerations it appears that a scheme involving the primitive variables P and V that are calculated at the center of the control volume will, if at all, converge to a solution that is a superposition of the real solution and an arbitrary amount of the "null solutions" for velocity and pressure as shown above.

To solve both the difficulties mentioned above (i.e., that of conservative fluid flow and of obtaining a sensible pressure field) we resort to the simple device of calculating the velocity field at sub-nodes positioned <u>on</u> the faces of the control volumes [A], [B], etc. in Figs. 3 and 4. Thus, for the one-dimensional system being described, <u>two</u> grids are used: the main grid nodes, centered in the control volumes [A], [B], etc., at which the pressure and temperature fields are evaluated; and a sub-grid of sub-nodes located midway between the nodes of the main grid for evaluating the velocity field only. The values of velocity evaluated at these sub-nodes will be the average value of the velocity of the

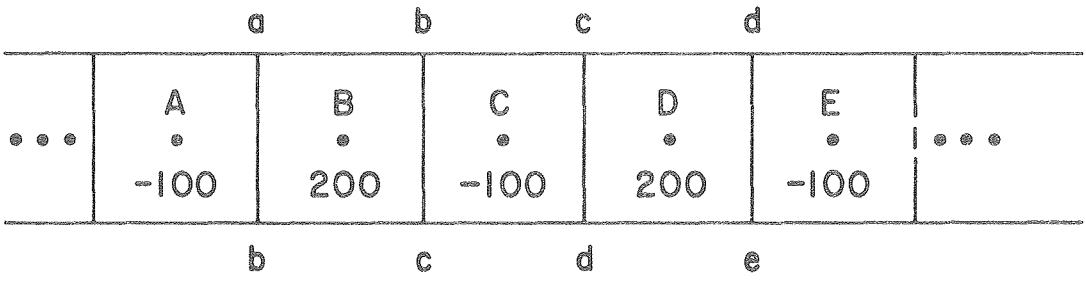

A HYPOTHETICAL PRESSURE DISTRIBUTION, IN A ONE-DIMENSIONAL GRID, WHOSE NET EFFECT ON THE CONTROL VOLUMES (CENTERED AROUND NODES A,B,C,...) IS EXACTLY ZERO, THOUGH SUCH A PRESSURE FIELD IS PHYSICALLY UNACCEPTABLE.

XBL 7911-13114A

Fig. 4

fluid contained in a control volume centered around the particular sub-node.

Thus, in Fig. 3 the outflow of fluid passing from [B] to [C] is simply the value of the velocity at the sub-node on the face *bc*. The problems arising from the averaging procedure used for calculating the velocity at the face thus disappear.

Similarly in Fig. 4, the pressure at nodes B and C drives the velocity control volume centered around the sub-node located on the face *bc*. Since this control volume has its faces passing precisely through nodes B and C, problems arising from the differencing procedure used for calculating the pressure difference across each face separately now disappear. The net pressure difference across the points B and C is exactly the pressure difference experienced by the fluid in the control volume centered on the sub-node on *bc*, and with faces passing through the nodes B and C.

This scheme is extended in three dimensions by having three separate sub-grids for the three components of the fluid velocity. The nodes of the sub-grid for the i^{th} component of velocity (i = 1, 2 or 3) are located midway between the nodes of the main grid and their neighbors in the i^{th} direction (i = 1, 2 or 3). Thus the u-components are calculated with a sub-grid using nodes u, d, etc. in Fig. 2; the v-components with a sub-grid with nodes at w, e, etc.; and the w-components with a sub-grid with nodes at s, n, etc. The details of the resulting grid scheme as shown in Fig. 5.

The equations for the velocity components [Eq. (3.11b)] are cast into finite difference form in precisely the same manner as described

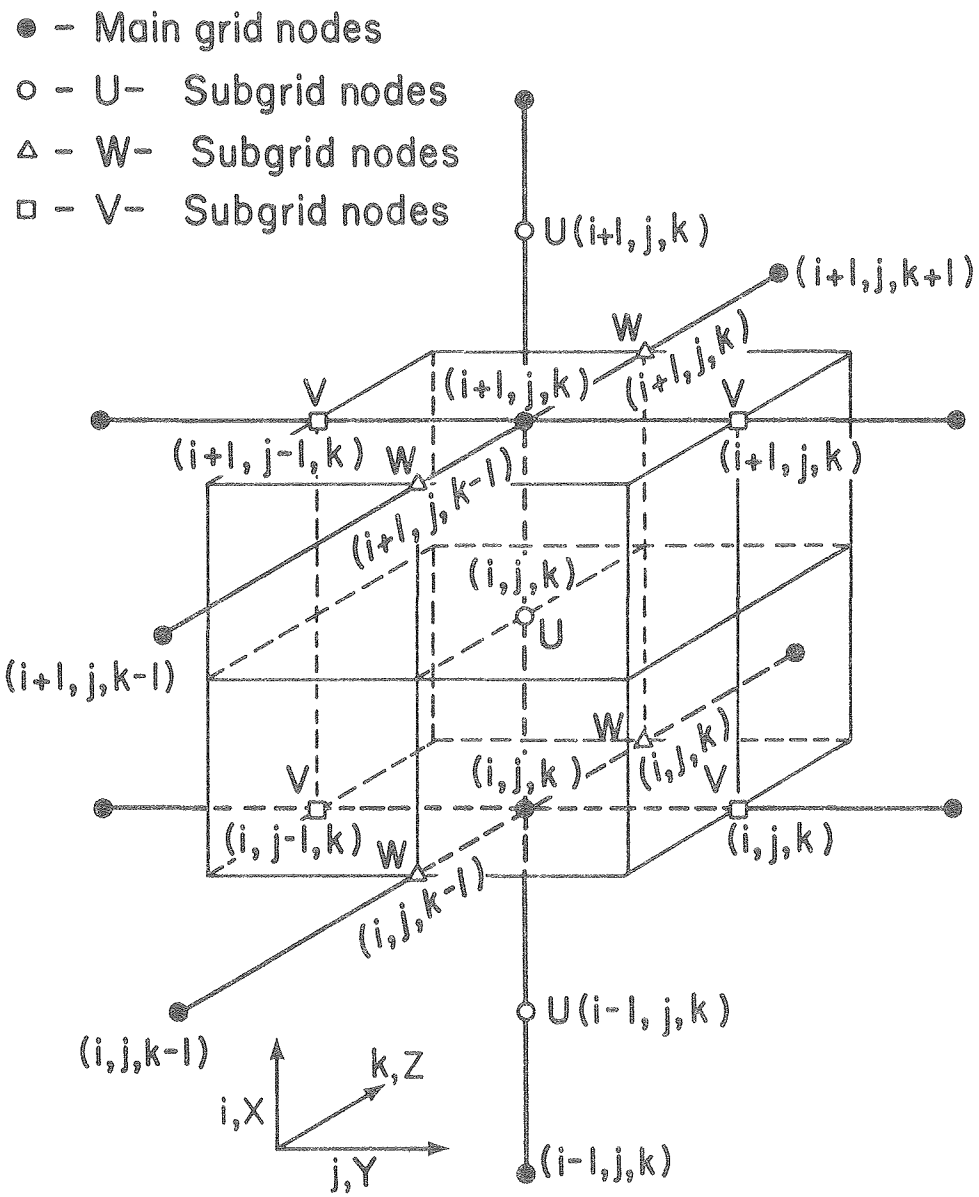

Fig 5. AN ILLUSTRATIVE GRID SECTION SHOWING THE AXES x,y,z; THE GRID INDICES i,j,k; AND THE RELATIVE POSITION OF THE MAIN GRID AND THE STAGGERED VELOCITY GRID NODES NEAR INDICES (i,j,k).

XBL 7910-13112

above for the energy equation; however, here one must also include the pressure derivative and the (buoyant) body force terms that are absorbed in the constant B in the equation like (3.14).

We now direct our attention to the calculation of the pressure field. The continuity equation (3.11a) is imposed on the velocity field as follows: $\nabla \cdot \vec{V} = 0$ integrated over the control volume in Fig. 2 yields

$$FU(U_e - U_w) + FE(V_n - V_s) + FN(W_u - W_d) = 0 \quad . \tag{3.16}$$

The pressure gradients are to be used to ensure that the velocity field obeys this condition.

Rewriting Eq. (3.11b) for the v-component evaluated at node e in Fig. 2 as

$$A_e \cdot V_e^* = FE \cdot (P_P^0 - P_E^0) + \text{other terms} \quad , \tag{3.17}$$

where V_e^* is the value of the V-component at node e to be evaluated, A_e is the coefficient of V_e^*, and FE is the area upon which the pressure difference acts. In solving Eq. (3.17) for V^*, we use the values of pressure obtained in the previous iteration (hence the "0" superscript). The result of solving this equation will be denoted by V^*. Similarly, we use U^* and W^* to denote the velocity components obtained by solving Eq. (3.11b) for the U and W components of velocity. Since any constraint of the type of Eq. (3.16) has not been imposed in solving for U^*, V^*, and W^* in this iteration, the velocity field obtained by U^*, V^*, and W^* does not satisfy the continuity equation, (3.16). They would do so if we had used correct (new) values of pressure in equations such as (3.17).

Denoting by P' the amount by which the P values were in error, i.e.,

$$P = P^0 + P' \tag{3.18}$$

where P is the "correct" pressure field which will produce velocity fields satisfying the continuity equation (3.11a). Notice that in Eq. (3.17) the velocity components U^*, V^*, and W^* are linearly dependent on P. So once we calculate P', it is easy to correct the velocity components by including the effect of P'. In fact, this is precisely the basis of calculating P' from U^*, V^*, and W^*. If we denote by U, V, and W the corrected velocity components, then, by Eq. (3.17), we have equations of the type

$$V_e = V_e^* + \frac{FE}{A_e}(P_P' + P_E') \quad , \tag{3.19}$$

where V_e are the correct velocity components. The equation (3.19) for U, V, and W can be substituted into Eq. (3.16) to obtain an equation for the P' field, Eq. (3.20) below.

If the coefficients (FE/A_e) appearing in the equations of type (3.19) are denoted by COFU for the U-field, COFV for the V-field, and COFW for the W field, and if the coefficients are subscripted by the notation of the nodes marked in Fig. 5, we obtain the equation for P' as:

$$\begin{aligned}
&[(COFU_u + COFU_d)FU + (COFV_e + COFV_w)FE + (COFW_s + COFW_n)FN]P_P' \\
&\quad = (COFU_u \cdot FU)P_U' + (COFU_d \cdot FU)P_D' + (COFV_e \cdot FE)P_E' \\
&\quad + (COFV_w \cdot FE)P_W' + (COFW_s \cdot FN)P_N' + (COFN_n \cdot FN)P_S' \\
&\quad + [FU(U_d^* - U_u^*) + FE(V_w^* - V_e^*) + FN(W_s^* - W_n^*)] \quad .
\end{aligned} \tag{3.20}$$

The constants COFU, COFV, and COFW defined above are evaluated during the calculation of the component fields U^*, V^*, and W^*. Thus Eq. (3.20) is enough to determine the pressure correction field P'. Solving this equation will yield a P' field which can then be used to obtain U, V, and W components satisfying (3.11a) via the U^*, V^*, and W^* components and equations like (3.19). This will yield a velocity field satisfying the continuity equation, (3.16).

C. The Method of Solution

The iterative method of solution of these equations is obviously preferred. Iterative methods can easily handle nonlinearities while maintaining the linearity of the equations to be solved in each iteration. They are much faster than the older direct methods (such as Cramer's rule or Gaussian elimination*) because they make use of the sparseness of the matrix of coefficients of the equations to be solved. (By sparse matrix we mean a matrix with a large number of elements being zero. This arises from the fact that in each different equation, only the field variables of neighboring nodes are involved.)

The Gauss-Seidel iterative method (see, e.g., Ref. 42) is relatively slow in its rate of convergence compared to the implicit alternating-direction method; especially for large values of N (Ref. 43). The alternating-direction method makes use of splitting the time-step to obtain the equations in a form which requires only the inversion of a

*To solve a system of 26 equations in 26 unknowns by Cramer's rule on a CDC-6600 would require an estimated 10^{16} years — a million times the present estimate of the age of the Universe.

tri-diagonal matrix.* This is extremely attractive since extremely fast algorithms for inversion of tri-diagonal matrices, popularly called TDMA (for Tri-Diagonal Matrix Algorithms), exist.

The ADI method, as applied to a rectangular grid in three dimensions, proceeds by splitting each time-step into three parts. The first sweep of the iteration begins by solving the equation [say, for the θ field, Eq. (3.11c)] for nodes on a single line parallel to the, say, x axis. The values of θ for all nodes along this particular line of the main grid are considered unknowns, while for all other grid-nodes, the values of θ obtained from the last iteration, denoted by θ^0, are used as the best estimate. The resulting set of linear algebraic equations (equal to IXMAX in number if there are IXMAX nodes along the x-direction) each contain only three unknowns; each equation involves three unknown values of θ on three consecutive neighboring nodes (along the line under consideration). The resulting set of equations, considered as a matrix equation, has a tri-diagonal matrix of coefficients which can be readily inverted to solve the equations. This procedure, when repeated for <u>each</u> line parallel to the x-axis in the three-dimensional rectangular parallelpiped grid, gives rise to an intermediate θ field, which we will call θ_1 here. (This field is intermediate because the ADI procedure has split the time-step, Δt, in three, and has advanced the θ field by only $\Delta t/3$ while solving Eq. (3.11c) along each line parallel to the x-axis.) Now using θ_1 as the best estimate, the nodes along each line of the grid parallel to the y-axis are updated, line by line, to the (split) time of $2\Delta t/3$ by advancing the calculation by another $\Delta t/3$ from θ_1. The newly

*A tri-diagonal matrix is a square matrix with only the main diagonal and the sub and super elements being non-zero.

obtained fields are denoted by, say, θ_2. The procedure is repeated, advancing field θ_2 by another $\Delta t/3$, this last time solving the tri-diagonal matrix equations formed by considering nodes along each line parallel to the z-axis, one line at a time. This brings the field θ^0 a full time-step Δt forward to the field θ. This advance was obtained by solving nothing more complicated than a simple tri-diagonal matrix, $3N^2$ times if there was a total of N^3 points in the three-dimensional grid. The time-step was split in three, and each substep was used to advance the field solving along lines parallel to a different axis.

This similar solution procedure is used to calculate fields U^*, V^*, and W^* mentioned in Eq. (3.20). The resulting fields are then used to formulate equations for the P' field, as defined in Eq. (3.20).

The P' field is solved next, again using the ADI procedure for a rapid solution. The initial "best" estimates of P' required in the evaluation of P' by ADI is zero everywhere. This P' is then added to the old value of P (denoted by P^0), to obtain the new value of P field [Eq. (3.18)]. This value of P' is also used to obtain the corrected value of the velocity-component field via equations like (3.19), from the U^*, V^* and W^* fields.

The calculational sequence is thus as follows:

(1) Read in the boundary conditions, fluid properties, grid locations, and time step size.

(2) Construct sub-grids for velocity components.

(3) Initialize values of the fields.

(4) Calculate the temperature field at the main grid nodes by solving the energy equation (3.11c) for time step size Δt.

(5) Calculate the intermediate velocity components U^*, V^*, and W^* at the nodes of their sub-grids by solving the momentum equations (3.11b) for a time step Δt.

(6) Calculate the pressure correction P' needed to make the velocity field satisfy the continuity equation (3.11a) by solving Eq. (3.20).

(7) Using P', obtain the velocity components U, V, and W via equations like (3.19). This is the new velocity field for this time step.

(8) Update the pressure field by Eq. (3.18).

(9) Check for convergence by calculating the fractional change in the field values from the last iteration. If convergence is not yet obtained, go back to step (4).

3.5 Boundary Conditions

The boundary conditions, described below, are handled by constructing the grids as depicted in Fig. 6 (in this figure, the z-dimension has been suppressed for the sake of clarity). Notice that the main grid nowhere coincides with the physical boundary and always has one plane (the line in Fig. 6) of main grid nodes on the other side of the physical boundary by a half cell-length.

The velocity component sub-grids are constructed in such a way that each of the physical boundaries of the (rectangular) space under study coincides with an edge of the sub-grid for the velocity component normal to that boundary. For example, in Fig. 6 the sub-grid for the U-component has its lower edge coinciding with the physical boundary normal to the

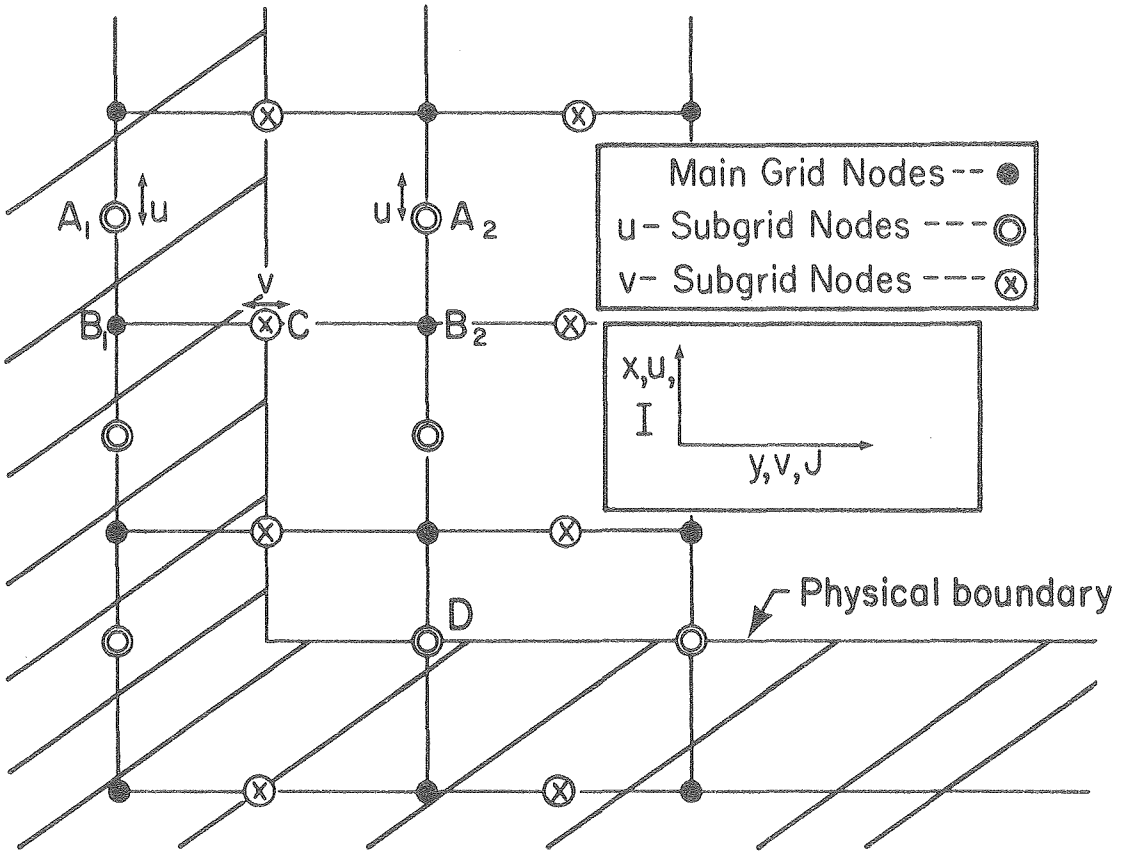

Fig 6. DETAILS OF GRID NEAR A CORNER OF THE PHYSICAL BOUNDARY. Z DIMENSION HAS BEEN SUPPRESSED FOR CLARITY. THE GRID PENETRATES INTO THE PHYSICAL BOUNDARY BY A HALF CELL-LENGTH.

XBL7910-13110B

X-axis, while the edge of the sub-grid for the V-component coincides with the physical boundary normal to the Y-axis.

The following method of imposing the prescribed boundary conditions is used for calculations of θ, U^*, V^*, W^*, and P':

(1) The user-specified values of θ at the physical boundary are ensured by requiring, in each iteration, that the average of the value of θ at the two main grid nodes bracketing the particular region of the physical boundary equals the value prescribed at that region of the physical boundary. In Fig. 6, for example, the values of θ calculated at nodes B_1 and B_2 will be required to average to the (user-prescribed) value of θ at the boundary region C bracketed by nodes B1 and B2. This procedure has an additional advantage for calculating the temperature gradient at the physical boundary (point C in Fig. 6) by simply differencing the value of θ calculated for nodes on either side of the boundary (nodes B1 and B2 in Fig. 6).

(2) The prescribed velocity boundary conditions for each component are imposed in the same manner as described above whenever the sub-grid for that component does not coincide with that physical boundary. In Fig. 6, if the boundary value of the U-component (specified on the physical boundary parallel to the X-axis) is zero, the calculational procedure ensures that at each iteration the average of the values of U^* (and U) calculated at sub-grid nodes A_1 and A_2, always equals zero.

In those cases when the particular sub-grid nodes coincide

with the physical boundary (for example, the sub-grid for U components and the physical boundary normal to the X-axis in Fig. 6), the prescribed values of the component at the physical boundary are used for the values of the component at the coincident nodes (node D in Fig. 6).

(3) In calculating the P' field, the boundary condition is imposed (in the calculations) that the gradient of P' normal to the physical boundary should equal zero. This boundary condition is used only for calculating flows inside completely closed enclosures, or inside enclosures with specified inlet and outlet velocity conditions. For enclosures with specified inlet and outlet pressure conditions, this boundary condition is modified to take into account the prescribed values.

CHAPTER 4

VALIDATION OF THE NUMERICAL SCHEME

4.1 Introduction

This chapter describes the comparisons of the calculational results of the numerical scheme described in the last chapter with various published numerical and experimental results.

The problems of convective heat transfer in buildings are often essentially three-dimensional in nature (i.e., they exhibit kinds of behavior that cannot be reproduced in a two-dimensional simulation). Thus a three-dimensional code is essential for proper simulation of many representative situations. Historically, however, a large amount of work has been done on relatively simpler, two-dimensional problems. Thus there is a substantial body of published numerical and experimental research on two-dimensional enclosure flows. This provides the ease of testing the written code against published data. Also, in terms of writing the code, it was expedient to write, debug and test the two-dimensional code first. Based on the experience gained in this effort, the three-dimensional version of the code was written.

4.2 Mechanically Driven Flows

The first tests, for the simplest flow situation, were conducted to ascertain that the programs converged to the expected fields, and that they produced residues of the order of the machine accuracy. These tests produced satisfactory results, converging to residues of the order of 10^{-15} (on CDC-7600 at LBL).

Donovan (Ref. 44) has carried out a numerical and experimental study of two-dimensional mechanically driven recirculating flow. The flow is induced in a square cavity by tangential motion of one of the walls of the cavity. The arrangement is schematically shown in Fig. 7. The velocity of the top plate is so arranged that the value of the Reynold's number, with respect to the side of the square, is 100. Donovan has also calculated the velocity and pressure fields for this problem by solving the Navier-Stokes equations for a 20×20 grid.

The profile of the vertical component of velocity along a horizontal line through the vortex center is shown in Fig. 8 for grid sizes of 10×10, 14×14, and 16×16. The continuous line is from Donovan's calculations; the points are calculated using the code described herein.

Figure 9 shows the comparison of the results of the code with Donovan's calculations for horizontal component of velocity along a vertical line through the vortex center, for grid sizes of 10×10, 14×14, and 16×16. The position of the vortex center, from Donovan's calculations, is at ($x = 0.75$, $y = 0.62$) where the x-y axes are as defined in Fig. 1. The vortex position calculated for the 16×16 grid was ($x = 0.73$, $y = 0.60$); the agreement is very good.

This test simply confirms that the code calculates the flow fields outside the boundary layer with good accuracy (the boundary layer in the situation described in Fig. 7 extends about 10% of the width of the cavity, from each wall. Recall the relation for flat plate laminar boundary layer thickness,

$$\frac{\delta}{L} \sim \frac{1}{\sqrt{Re}}$$

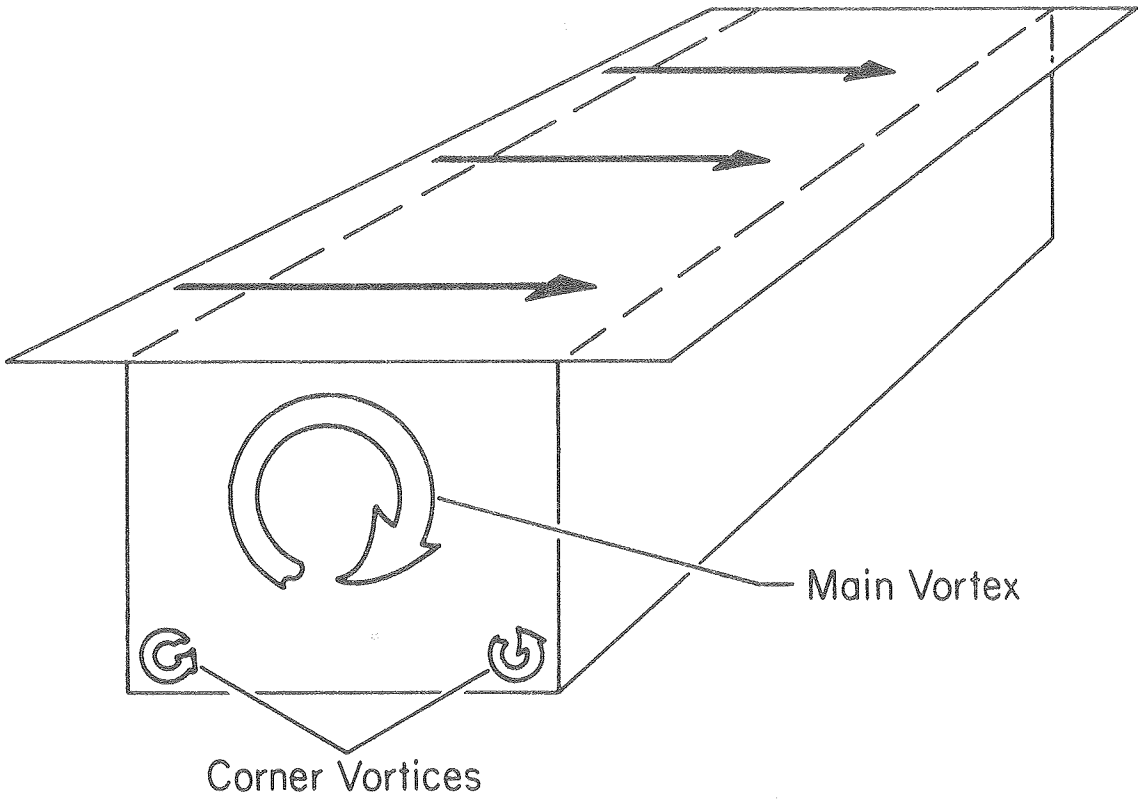

RECIRCULATING FLOW INDUCED IN A FLUID INSIDE A SQUARE CAVITY BY TANGENTIAL MOTION OF ONE WALL.

XBL7911-13119

Fig. 7

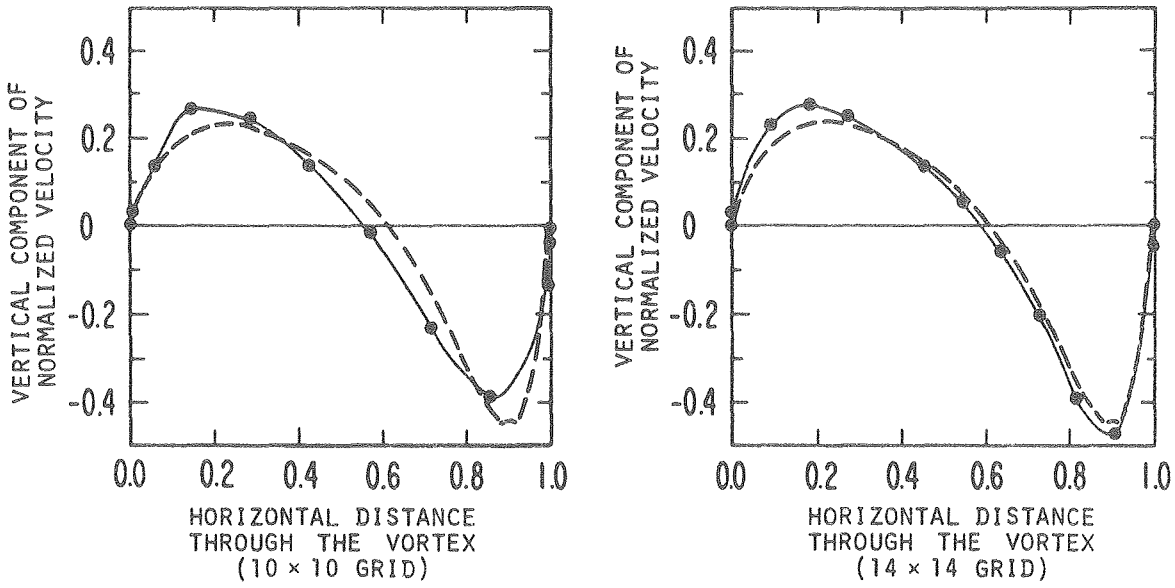

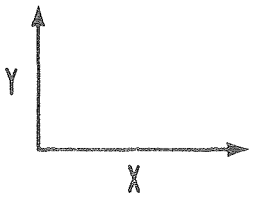

VERTICAL COMPONENT OF VELOCITY (Y-AXIS) ALONG HORIZONTAL DISTANCE THROUGH THE VORTEX CENTER (X-AXIS).

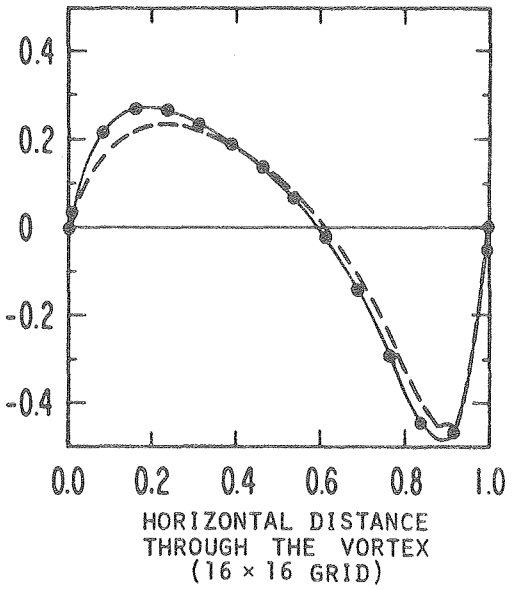

XBL7911-13121

Fig. 8

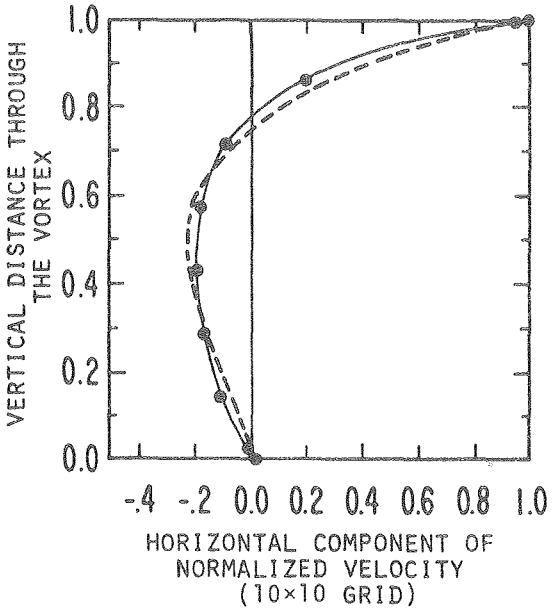

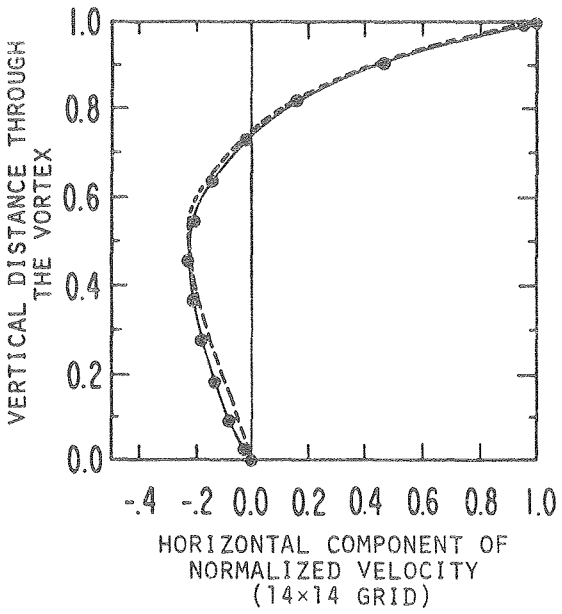

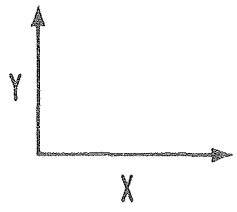

HORIZONTAL COMPONENT OF VELOCITY (X-AXIS) ALONG VERTICAL DISTANCE THROUGH THE VORTEX CENTER (Y-AXIS).

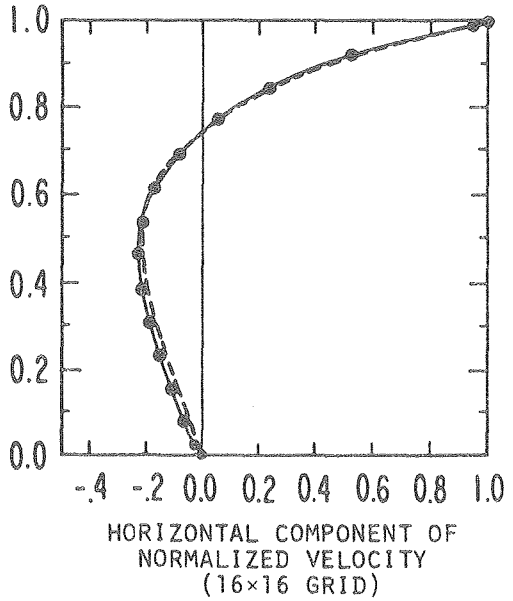

XBL7911-13122

Fig. 9

where δ is the boundary layer thickness and L is the distance along the plate from its leading edge. The corner vortices observed by Donovan (see schematic in Fig. 7) also show up in all the three grid sizes described here.

4.3 Buoyancy Driven Flows at Low Rayleigh Numbers

We next consider the problem of buoyancy-induced flows. de Vahl Davis (Ref. 45) has used a 10×10 grid to solve the Navier-Stokes equations for a fluid inside a square cavity. The (opposite) vertical walls of the cavity are maintained at constant temperature, while the ceiling and the floor of the cavity have a linear surface temperature profile. Figures 10, 11 and 12 show the results of this code compared with the results of de Vahl Davis, for three different Rayleigh numbers, for local Nusselt number as a function of distance along the cold wall. The smooth line shows the results of de Vahl Davis, the dotted line shows the results of the present numerical scheme.

It is to be noted that de Vahl Davis has used an evenly spaced 10×10 grid, and then used a forward differencing procedure to calculate the local Nusselt numbers at the wall. His temperature grid coincides with the boundary of the cell at the edges, so the nearest temperature node in the direction normal to the boundary is at a distance equalling 10% of the cavity size. In contrast, the grid system used here (see Fig. 6) allows evaluation of the temperature gradient at the boundary without using a forward differencing procedure. Besides, the results displayed here have been calculated with 15×15 grid size, with a smaller grid spacing near boundaries than in the central region; this allows

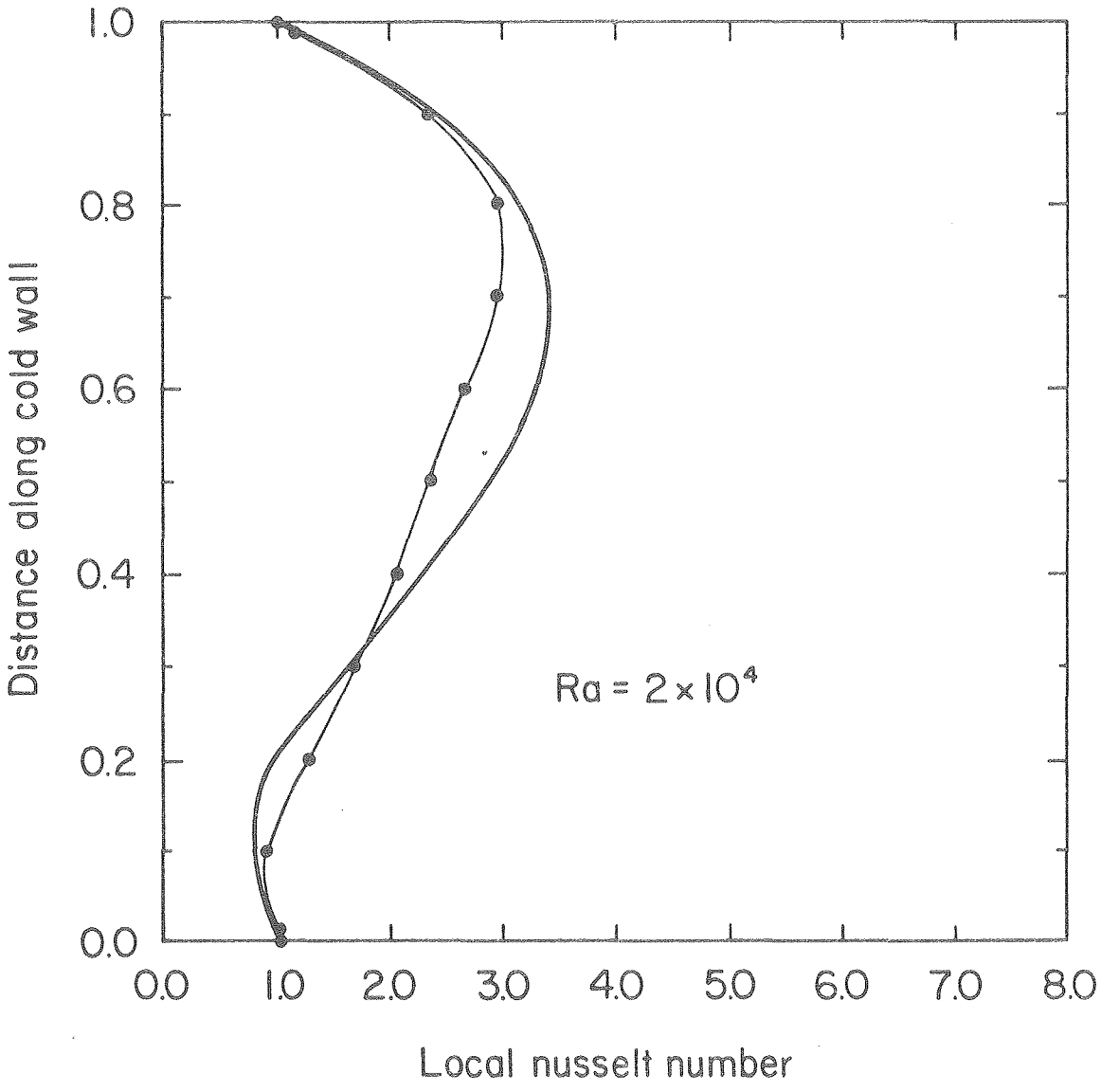
1.0
0.8
0.6
0.4
0.2
0.0
Distance along cold wall
Ra = 2×10⁴
0.0
1.0
2.0
3.0
4.0
5.0
6.0
7.0
8.0
Local nusselt number
XBL7911-13116

Fig. 10

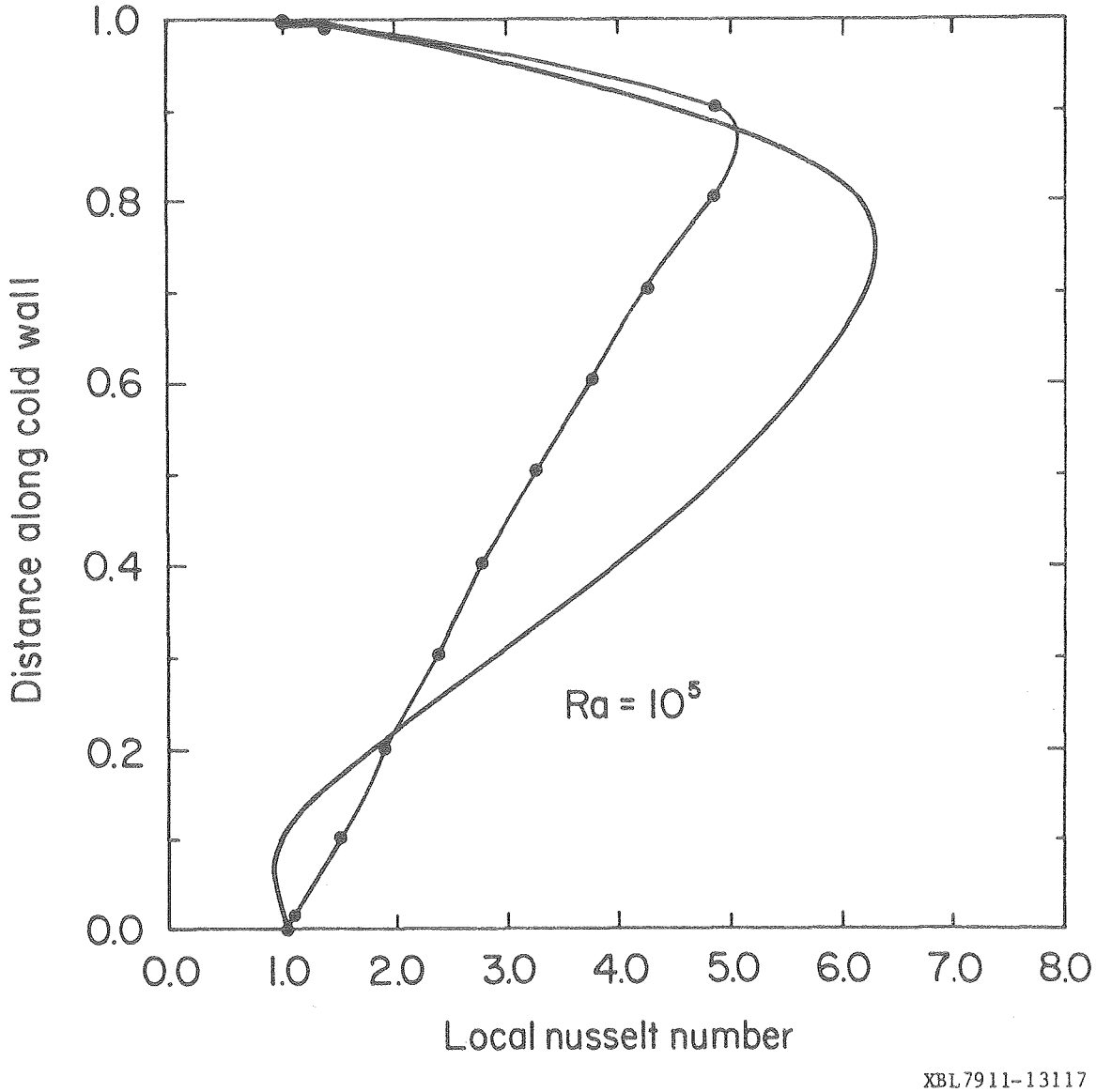
1.0
0.8
0.6
0.4
0.2
0.0
Distance along cold wall
Ra = 10^5
0.0
1.0
2.0
3.0
4.0
5.0
6.0
7.0
8.0
Local nusselt number
XBL7911-13117

Fig. 11

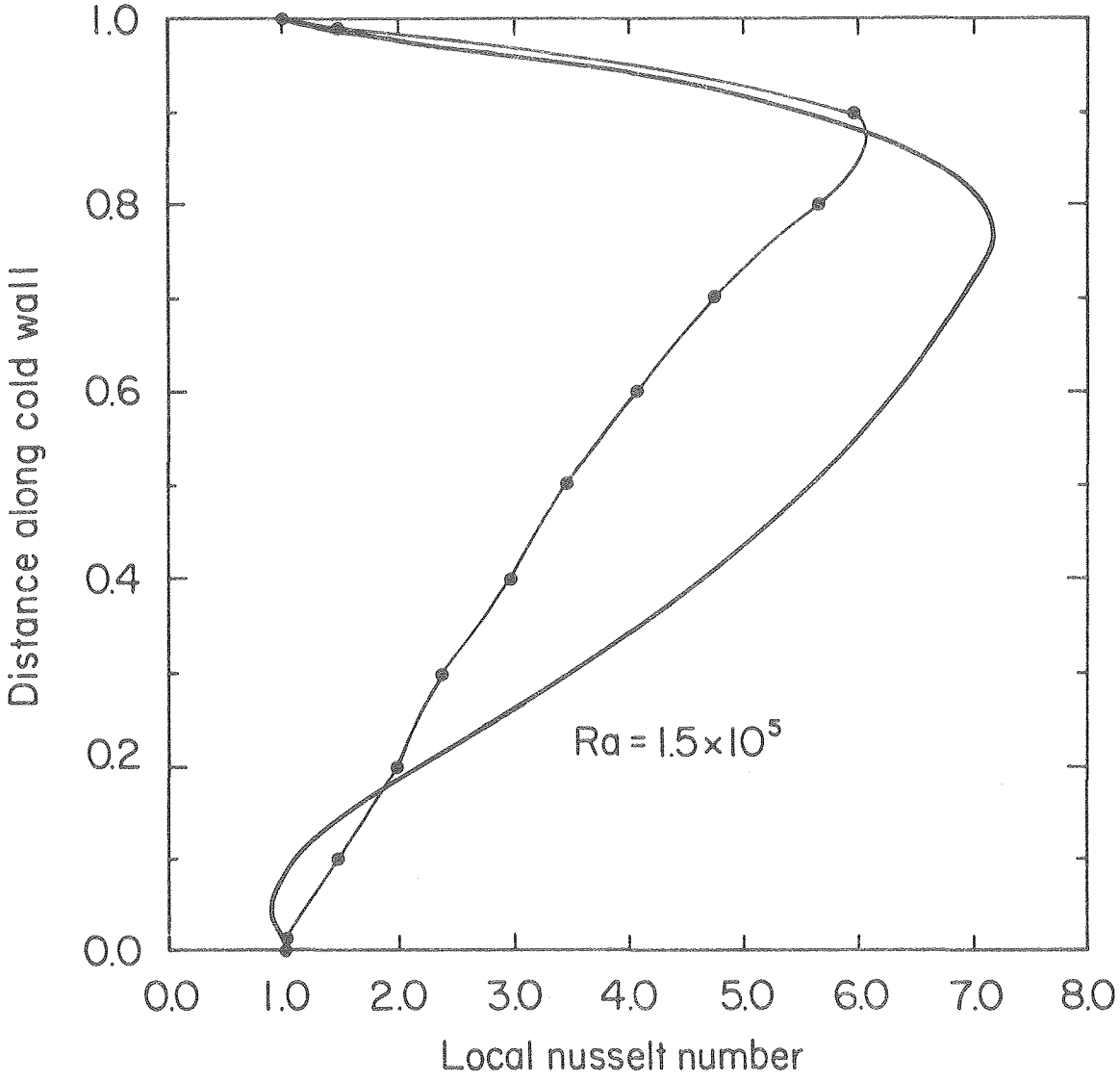

XBL7911-13118

Fig. 12

better representation of the sharp changes in velocity and temperature near the boundary layer. (For this problem, the boundary layer regime starts for $Ra > 10^4$, which is the case here.)

For the same reason, de Vahl Davis calculates the local Nusselt number at the top and bottom of the cold wall to be identically equal to 1.0 (see Figs. 12-14). This results from the temperature node being situated exactly at the end of the wall, the nearest temperature node along the wall again being 10% of the wall-length away. The calculations with the code described here do not have this limitation. This is the reason why the local Nusselt numbers calculated by this code are different from the 1.0 calculated at the two ends of the wall.

Notice that for 15×15 grids, two grid lines are outside the physical boundary (see Fig. 6), two more grid lines are each in the boundary layer; the cell size inside the volume of the cavity is therefore the same as for de Vahl Davis, $(1/10 \times 1/10)$. The computation for each run took ~31 seconds to reach residues of 10^{-7} for the velocity fields.

4.4 Comparisons at Higher Rayleigh Numbers

The flow induced in a two-dimensional square cavity, with adiabatic ceiling and floor, and with isothermal vertical walls maintained at different temperatures, is considered next. The situation under study is schematically shown in Fig. 13.

A quantity of most interest in this problem is the Nusselt number. Recall that the Nusselt number is a measure of the relative strengths of the convective and conductive heat transfer processes. Note that by

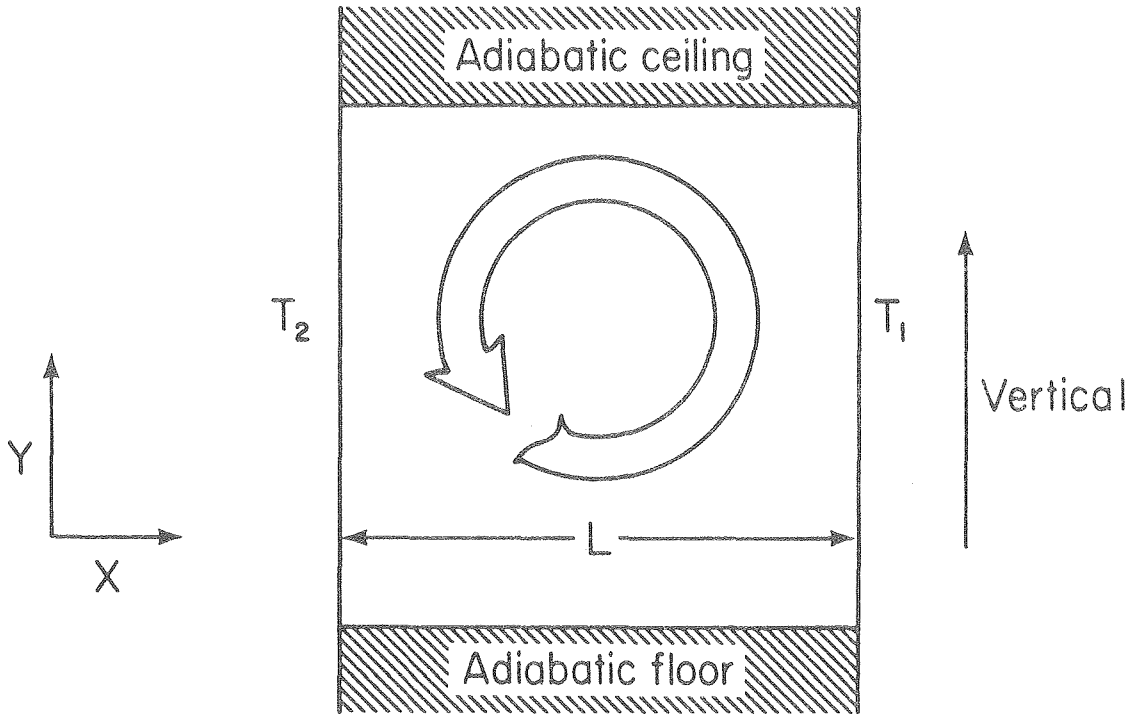

Fig 13. RECIRCULATING FLOW INDUCED IN A FLUID INSIDE A TWO-DIMENSIONAL SQUARE CAVITY, DEFINED BY ADIABATIC FLOOR AND CEILING AND ISOTHERMAL WALLS, AT TEMPERATURES T_1 AND T_2 ($T_1 > T_2$).

XBL7911-13124

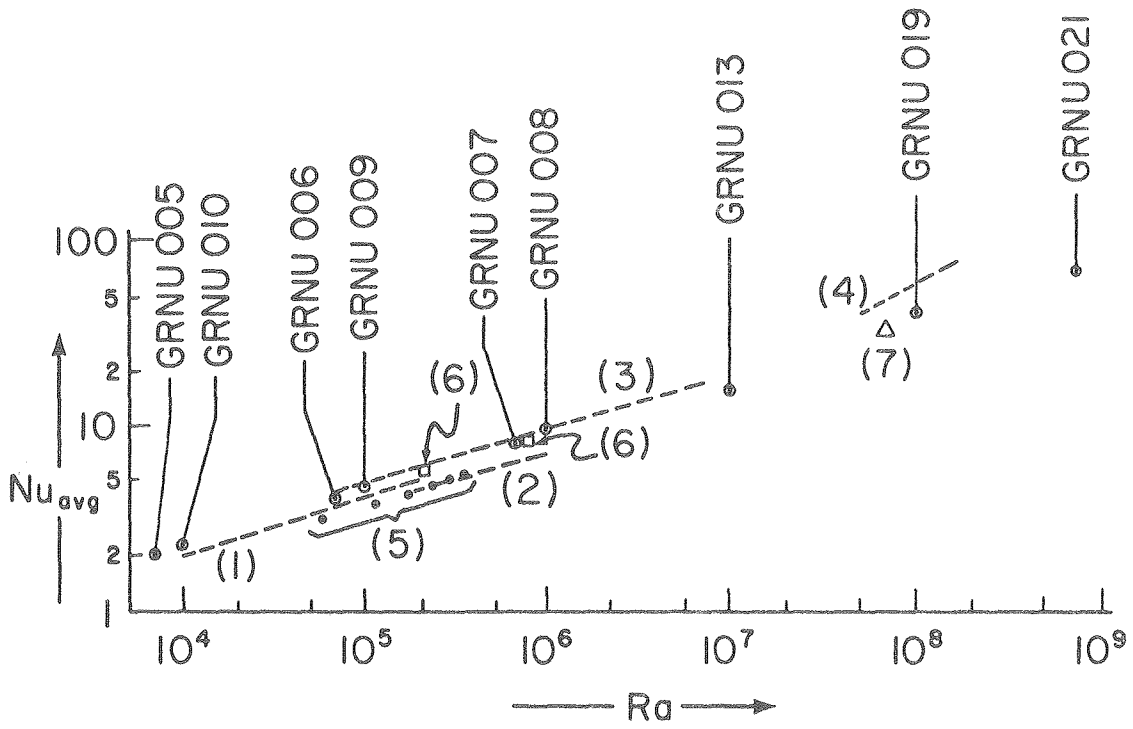

CURVE (1): de VAHL DAVIS CALCULATIONS (Ref. 46)

CURVE (2): FROM RESULTS OF EMERY, EXPERIMENTAL (Ref. 47)

CURVE (3): PORTIER et al., CALCULATIONS, Pr = 0.7 (Ref. 48)

CURVE (4): BURNAY et al., DATA REDUCED FROM EXPERIMENTS, Pr = 0.7 (Ref. 49)

RESULTS (5) ARE FROM RUBEL AND LANDIS, CALCULATIONS (Ref. 50)

RESULTS (6) ARE FROM QUON, CALCULATIONS (Ref. 51)

RESULT (7) IS FROM FROMM (Ref. 52)

POINTS INDICATED BY ⊙ ARE FROM GADGIL (THE INDICES GRNUnnn REFER TO THE COMPUTER PRINTOUTS ON FILE)

Fig 14. DEPENDENCE OF $\overline{Nu}$ ON Ra, FOR TWO-DIMENSIONAL FLOW INSIDE A SQUARE CAVITY. COMPARISON WITH PUBLISHED RESULTS.

XBL7911-13125B

definition, the Nusselt number is independent of the thermal conductivity of the working fluid, and also independent of the actual temperature drop involved. It is, instead, strongly dependent on the development of the fluid flow:

$$Nu = \frac{L}{(T_{max} - T_{min})} \left.\frac{\partial T}{\partial X}\right|_{\substack{\text{normal to} \\ \text{the boundary}}}$$

For a solid or other pure conduction problem, the Nusselt number will remain the same for a given distribution of boundary temperatures, independent of the actual magnitude of $(T_{max} - T_{min})$ involved. This is to say, the conductive heat transfer from a boundary will be simply linearly proportional to the magnitude of $(T_{max} - T_{min})$ for an ordinary solid.

On the other hand, for a problem involving both convection and conduction, such as the one described in Fig. 15, the convective flow brings cool fluid near the hot wall and warm fluid near the cool wall. The strength of this convective flow directly depends on the magnitude of $(T_{max} - T_{min})$, on the Rayleigh number, in fact. Thus, larger values of $(T_{max} - T_{min})$, inducing larger fluid recirculation, actually increase the value of the Nusselt number. The Nusselt number then actually increases with the magnitude of $(T_{max} - T_{min})$, i.e., with increasing Rayleigh number. The heat transfer from a boundary is a highly nonlinear function of the magnitude of $(T_{max} - T_{min})$. Thus the dependence of the Nusselt number of the Rayleigh number is a measure of the development and character of the flow. The average Nusselt number, defined as

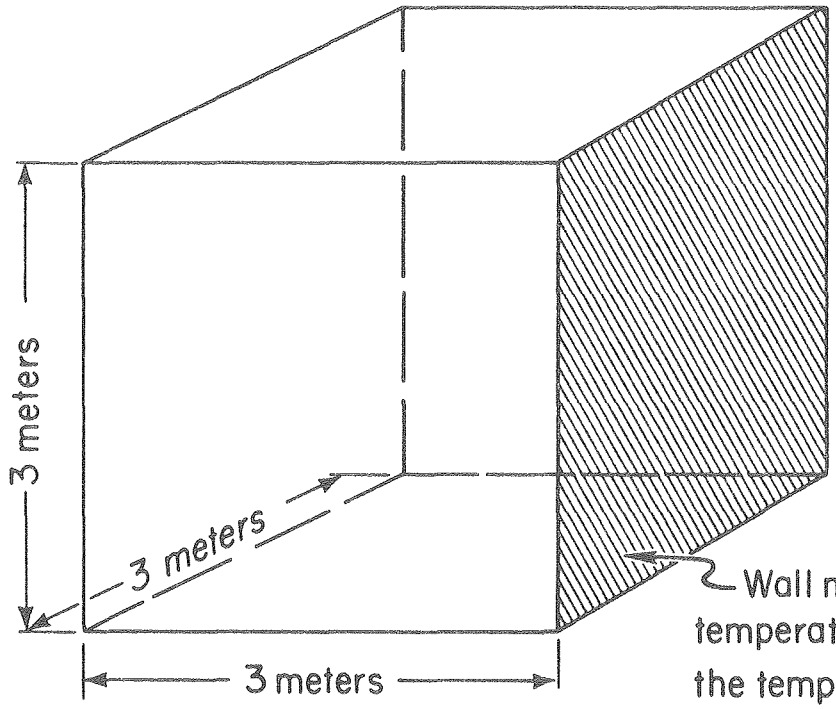

70	70	70	70	70	70
87	87	87	87	87	87
103	103	104	104	103	103
123	123	123	123	123	123
151	151	151	151	151	151
256	256	257	257	256	256

Variation of local convective Nusselt number on the surface of the hot wall.

XBL7911-13134

Fig. 15

$$Nu_{avg} = \frac{L}{(T_{max} - T_{min})} \int_0^L \frac{\partial T}{\partial x}$$

is plotted as a function of Rayleigh numbers in Fig. 14. On the same graph, we have superimposed relevant results of various investigators, both numerical and experimental (Refs. 46-52). The agrement is good. All the results of the code described here were calculated using the same 17×17 grid, and were run to convergence. For Rayleigh numbers of 10^7 or less, the runs converged in 20 seconds on the CDC-7600 at LBL. The runs for higher values of Rayleigh numbers were carried to 40 seconds.

4.5 Convective Heat Transfer from the Vertical Wall of a Three-Dimensional Enclosure

The three-dimensional code was used to simulate the air circulation in the situation illustrated in Fig. 15. The cube-shaped enclosure has one of its vertical surfaces maintained at a uniformly higher temperature than the other five surfaces. The Grashof number resulting for a temperature difference of 4.5°C and an enclosure size of 3 m^3 is 1.6×10^{10}. Figure 15 also shows the distribution of the local Nusselt number on the surface of the warm wall. The average Nusselt number for the wall was calculated to be 145.

In the engineering literature there is very little published data regarding experimental or numerical investigation of enclosure flow at Grashof numbers exceeding 10^7. However, it is possible to estimate the Nusselt number for the problem under consideration by noting the following two points:

(a) The air circulation induced by a hot vertical surface inside an enclosure is in many ways similar to the air movement induced by a free-standing vertical hot plate immersed in a bath of still fluid. The air circulation inside the enclosure, however, encounters much more viscous drag (due to all the other walls) than is the case for a free-standing vertical hot plate. One result of this several-fold increase in the viscous drag is that the Nusselt numbers (based on enclosure height and total height of the free-standing vertical plate) for the enclosure are consistently lower than those for a free-standing vertical plate by 40-50%. This is illustrated in Fig. 16, which shows the Nusselt numbers for free-standing vertical plates and for enclosures, in the range recommended by Kreith (Ref. 53).

(b) The other effect of the increased viscous drag on air circulation inside the enclosure is the increased stability of the flow. For a free-standing vertical wall, the regime of transition from laminar to turbulent flow is observed to be at Grashof numbers from 10^8 to 10^{10}. Beyond the Grashof number of 10^{10}, the flow is turbulent. For flow inside an enclosure, however, the transition regime goes up to a Grashof number of 3×10^{10}, as seen, for example, in videotapes of Ruberg's experiment (Ref. 54). From the physical interpretation of the Grashof number, this is understandable; recall that the Grashof number is the square of the ratio buoyant to viscous forces. For a four-fold (or six-fold) increase in the viscous forces, one can expect roughly one order of magnitude

Data referred from Kreith, (p 393, 402).

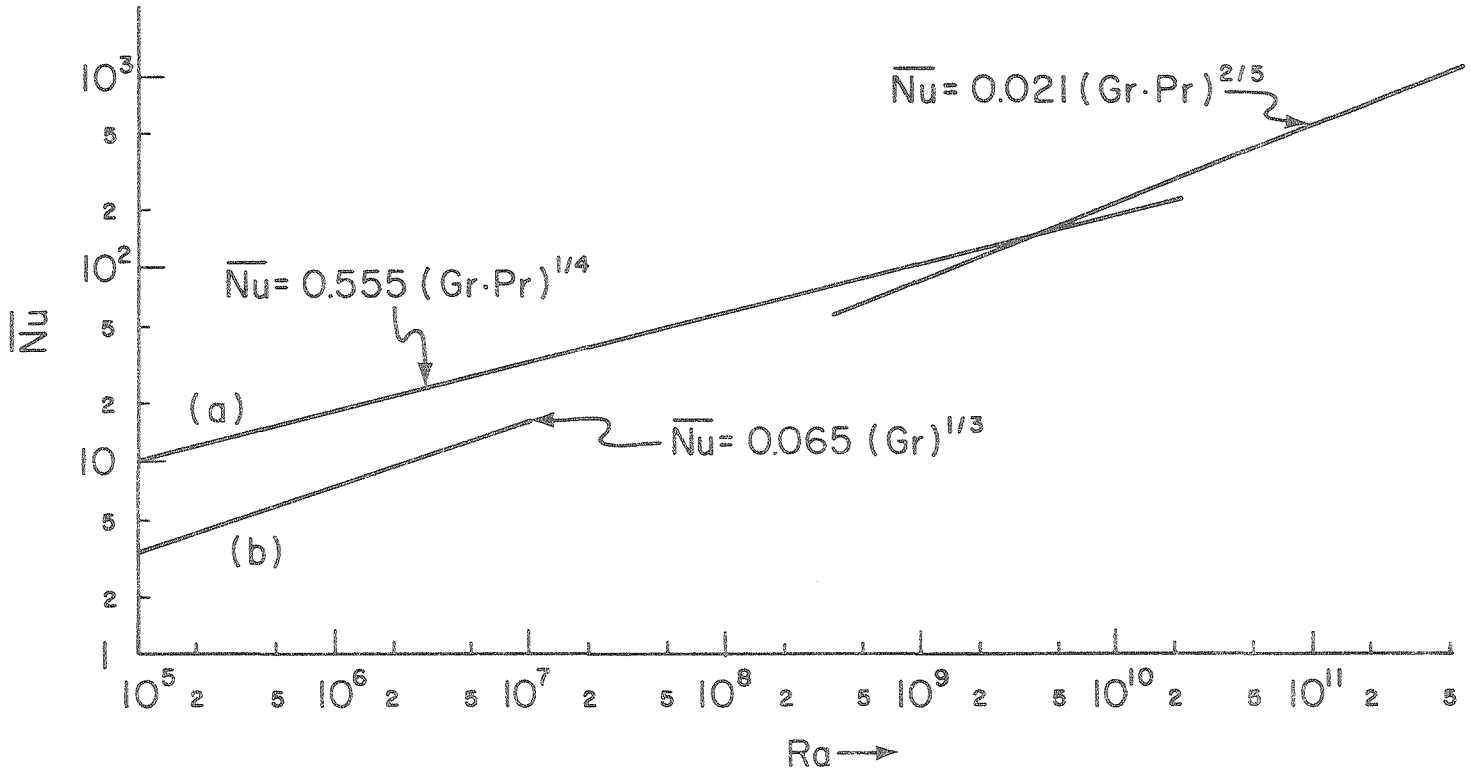

Fig 16. Correlation of data for natural convection for (a) free-standing vertical plates and cylinders
(b) enclosures, Pr = 0.7

XBL7911-13135

increase in the critical Grashof number (before the onset of fully turbulent flow). Also note from Fig. 16 that the Nusselt number does not change discontinuously with the onset of turbulence.

For a Rayleigh number of 10^{10}, the Nusselt number for a free-standing vertical plate is in the turbulent regime and is about 210 (see Fig. 16). If one extends the laminar flow correlation for a free-standing vertical plate up to Rayleigh numbers of 10^{10}, the Nusselt number is seen to be about 175. (Extending the correlation for enclosure flows up to a Reynolds number of 10^{10} yields a Nusselt number of 158.) The predicted Nusselt number of 145 is thus seen to be 17% lower than the extrapolated value for laminar flow Nusselt numbers for a free-standing vertical plate, and within 9% of the extrapolated value for a laminar enclosure flow.

4.6 Comparison with a Full-Scale Experiment with Three-Dimensional Flow

In 1978, Ruberg reported on the full-scale experiment performed at the Massachusetts Institute of Technology, depicted in Fig. 17. A detailed description of the apparatus and the experiments is given in Ref. 54. Ruberg measured the temperature distribution inside the enclosure in plane AA of Fig. 17 by means of thermistors mounted on a movable, rail-mounted boom. He also made videotapes of the flow induced inside the enclosure using smoke and soap bubbles as tracers. The videotapes clearly show that the flow (at Grashof number of $\sim 1.6 \times 10^{10}$ based on enclosure height) is not yet turbulent, but shows oscillations typical of the transition regime. Unfortunately, only a few measurements of

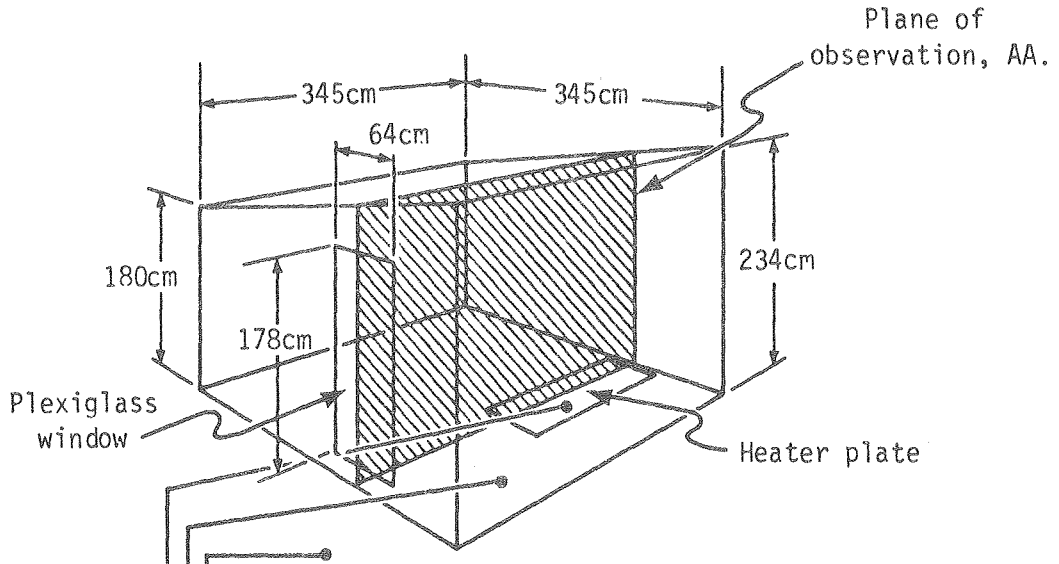

POSITION	C°	F°
Ambient air temperature	21.4	70.5
Room air temperature	40.6	105.1
Heater plate temperature	64.7	148.5

XBL7911-13133

Fig. 17

surface temperatures or surfaces other than the heater-plate and the window were made. So these temperatures have been estimated using available data.

Ruberg's measurements of air temperature were made in a way that could not exclude the effects of radiation. In particular, these effects are expected to bias the measured air temperatures directly above the heater plate towards higher values.

Three sets of isotherms produced for three sets of measurements of air temperatures in plane AA of Fig. 17 are shown in Fig. 18. The isotherms predicted by the computer code are shown in Fig. 19. In light of the limitations described above, the agreement appears satisfactory.

The computer runs predict a local Nusselt number for the hot plate based on room height of 180, implying a convective heat flux from the hot plate of 17.8 BTU-h/ft^2.

Ruberg has estimated the convective heat flux from the hot plate to be in the region of 27 BTU-h/ft^2. The computer prediction is lower than his estimate by 33%. Since the flow is in the transition regime, use of a model for buoyancy-induced turbulence would probably result in a better agreement. Such models are in an extremely early stage of development in the engineering literature, but can and should be incorporated into the code as they are developed and tested.

Isotherms measured in Ruberg's experiment

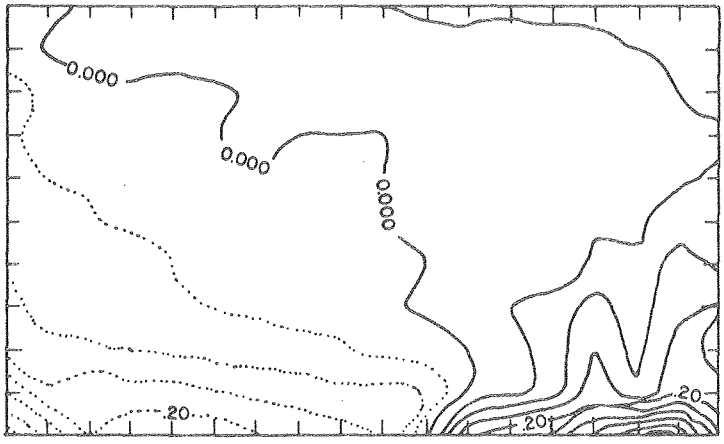

XBL 802-6638

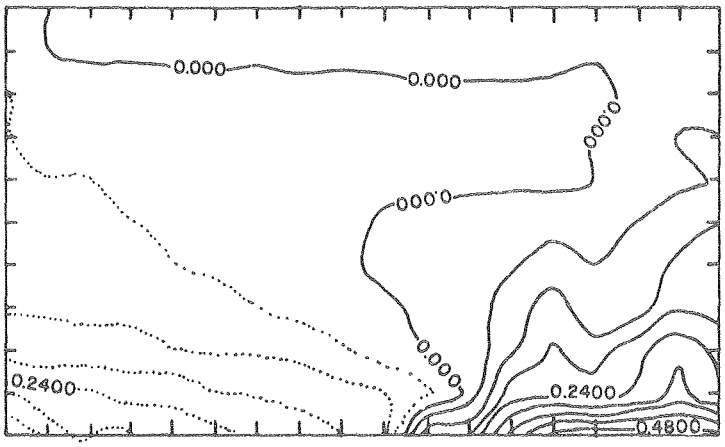

XBL 802-6635

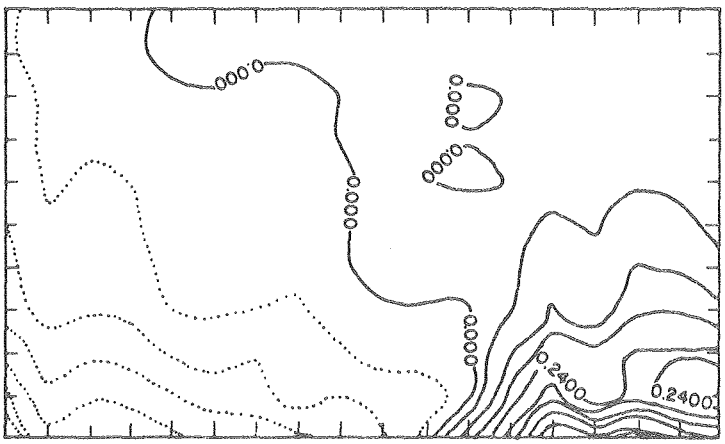

XBL 802-6637

Fig. 18

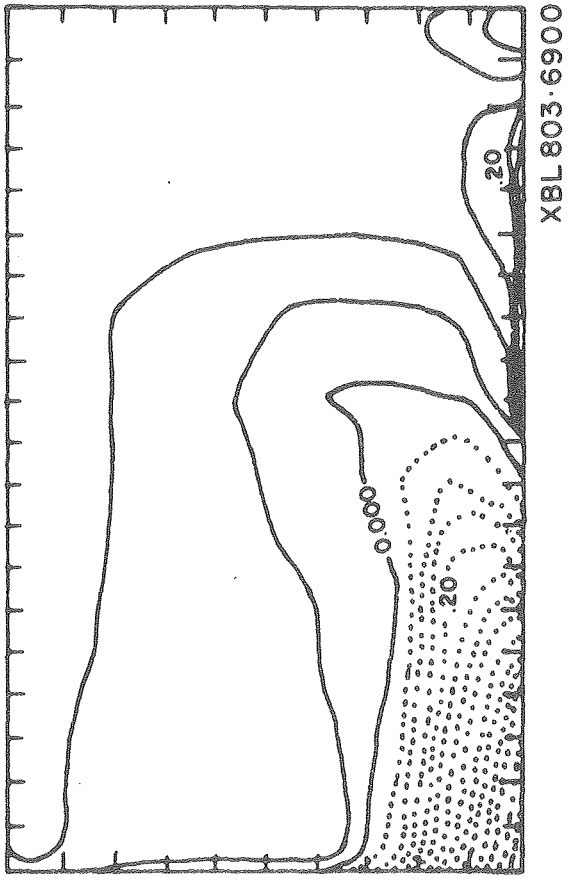

Numerically predicted isotherms for Ruberg's experiment.

Fig. 19

CHAPTER 5

AN ILLUSTRATIVE APPLICATION OF THE NUMERICAL CODE

5.1 Introduction

In this chapter, the computer code described earlier is used to investigate the effect of different distributions of incident solar energy in a direct-gain system, on the convective heat transfer from the walls and the floor.

5.2 Description of the Problem

Almost all of the public-domain computer programs for building energy analysis presently assume a uniform distribution of incoming solar energy on the interior surfaces of a room. Furthermore, all of them (with the exception of one version of BLAST (Ref. 7) which has not been released yet) assume the convective heat transfer coefficient to be a constant, independent of the surface temperature distribution.

To investigate the possible importance of the assumptions made about distribution of energy from sunlight on the internal surfaces with respect to convective heat transfer, the three situations illustrated in Fig. 20 were investigated. The three situations illustrate three different distributions of surface temperature possibly resulting from different assumptions about where the sunlight deposits energy. (The question is more complex than shown in Fig. 20 due to the conductive and radiative effects, but these are not taken up here.) Notice that in Fig. 20 the average temperature of each surface is the same for all the

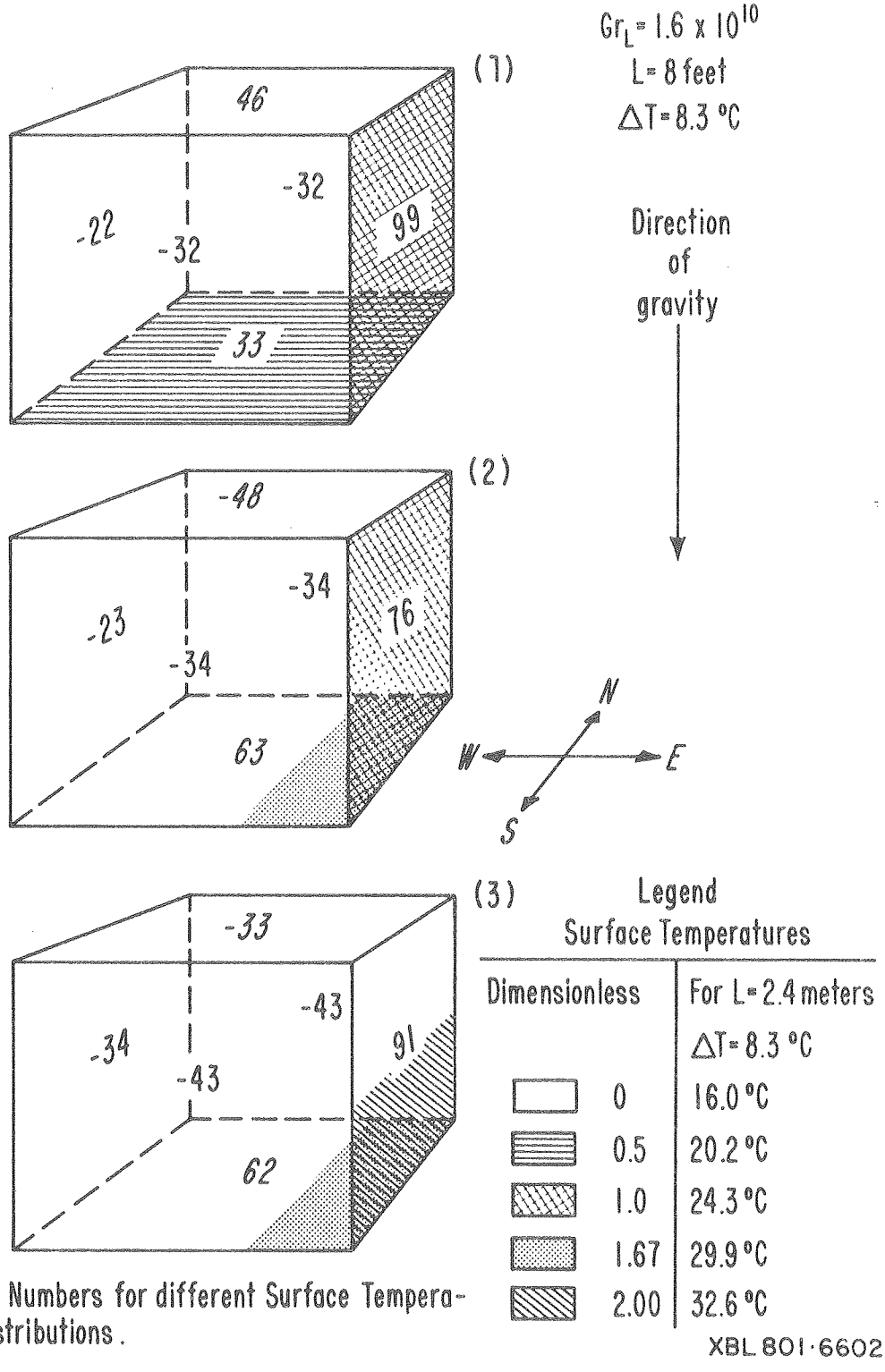

Nusselt Numbers for different Surface Temperature Distributions.

Fig. 20

distributions. The top illustration in this figure shows a hypothetical distribution resulting from an assumption of uniform distribution of solar energy on the entire floor. (The distribution can also be purposely produced by introducing a non-absorbing optical diffuser in the window.) The lower illustrations of Fig. 20 show hypothetical distributions of surface temperature corresponding to direct sunlight striking only a portion of the floor (and the wall).

5.3 Discussion of Results

The resulting convective heat fluxes from each surface are shown in Table 1 below. The room is assumed to be 2.44 meters (8 feet) to each side for calculating the heat fluxes. The surfaces are numbered in a manner consistent with Fig. 20. The surface temperature distributions are numbered (1, 2 and 3) consistently with the numbering used in the figure.

TABLE 1. Net convective heat fluxes (watts/m^2).

Temperature Distribution	East wall	West wall	North/South walls	Ceiling	Floor
1	8.8	-2.0	-2.9	-4.1	3.0
2	6.8	-2.1	-3.1	-4.3	5.6
3	8.1	-3.1	-3.8	-3.0	5.6

As one goes from distribution 1 to distribution 2, the convective heat fluxes from the west wall, the ceiling, and the north and south walls change by less than 10%. The heat extracted from the floor,

however, goes up from 3.0 watts/m^2 to 5.6 watts/m^2, an increase of 87%. At the same time, the heat extracted from the warm east wall drops from 8.8 watts/m^2 to 6.8 watts/m^2. This drop is, of course, due to the warmer air rising from the floor than was the case for distribution 1. The general character of the flow remains the same.

Going from distribution 2 to distribution 3, the character of the flow changes substantially. Due to the (relatively) cold upper half of the east wall, one observes a small loop of reverse flow in that region. The hot air from the floor and the lower half of the east wall rises away from the east wall, and a current of cool air descends from the top of the east wall to meet this rising hot air. The rising hot air mixes with this cool air and continues to rise towards the ceiling. Near the ceiling, a small part of the rising air turns eastward to feed the downward loop along the east wall, while the major portion moves westward to descend down the west wall.

The net heat flux from the east wall increases from 6.8 watts/m^2 (for case 2) to 8.1 watts/m^2. As a result of the different character of the flow discussed above, the heat deposited in the ceiling drops from 4.3 watts/m^2 to 3.0 watts/m^2, while the heat deposited on the west wall increases from 2.1 watts/m^2 to 3.1 watts/m^2. Since the upward moving warm air now separates from the east wall and moves westward at the halfway point, somewhat more heat is deposited on the north and south walls, too, the fluxes going up from 3.1 watts/m^2 to 3.8 watts/m^2. The heat extracted from the floor remains unaltered (from distribution 2) at 5.6 watts/m^2.

5.4 Conclusions

The convective heat transfer from the surfaces of an enclosure is seen to be strongly affected by the actual distribution of surface temperature (rather than merely the averaged surface temperature), which is decisive in determining the character of the flow. The effects are of the order of 100% for two different plausible distributions of surface temperatures.

The results summarized in Table 1 point towards important conclusions for a more efficient storage of direct gain solar heat in a thermally massive floor or wall. Intentional introduction of an optically non-absorbing diffuser in the glazing of a direct-gain system seems to have a significant effect on reducing the solar heat immediately deposited in the air.

The computer model described in these chapters predicts buoyant flows inside enclosures with fair accuracy (within 30%) up to Grashof numbers of 3×10^{10}, when compared with experimental data. The model can be used for investigating convective phenomena in buildings and for identifying strategies leading to improved thermal performance of buildings.

REFERENCES

1. Honma; Ph.D. Thesis, Royal Institute of Technology, Stockholm, Sweden (1975).
2. Nielsen; Ph.D. Thesis, Technical University of Denmark (1974).
3. NECAP Engineers Manual, U.S. Dept. of Commerce, Report N76-10752 (1975).
4. Lokmanhekim, Rosenfeld and Leighton; in Proceedings of the Third International Symposium on the Use of Computers for Environmental Engineering Related to Buildings, Banff, Alberta, Canada (May 1978).
5. DOE-2 Users Guide, LBL-8689 (February 1979).
6. Kusuda; National Bureau of Standards, NBS Building Science Series 69 (1976).
7. BLAST is copyrighted by the Construction Engineering Research Laboratory, U.S. Dept. of the Army, Champaign, Illinois.
8. Gadgil, Goldstein, Kammerud and Mass; LBL-9293 (1979).
9. Carroll; LBL-9270 (June 1979).
10. Goldstein; Ph.D. Thesis, Dept. of Physics, U.C.Berkeley (November 1978).
11. Sonderegger; Ph.D. Thesis, Dept. of Aerospace and Mechanical Sciences, Princeton University (September 1977).
12. Ruberg; M.S. Thesis, Dept. of Architecture, Massachusetts Institute of Technology (September 1978).
13. Casperson and Hocevar; Dept. of Energy Report DOE/CS/34145-1 (May 1979).
14. Akbari and Borgers/Borgers and Akbari; LBL-7802, LBL-8323 (1978 and 1978).

15. Burns, Chow and Tien; Int. J. Heat Mass Transfer 20, 919-926 (1977).

16. Balcomb's Test Cell descriptions.

17. Weber and Wray; in Proceedings of 4th National Passive Solar Conference, Kansas City (October 1979).

18. Third and Fourth National Passive Solar Conference Proceedings (1978 and 1979).

19. Spalding; Int. J. for Numer. Methods in Eng. 4, 551-559 (1972).

20. Reif; Statistical and Thermal Physics (McGraw Hill).

21. See e.g., Holman; Heat Transfer (McGraw Hill), p.217.

22. See Holman, Op.Cit., p.223.

23. Cheesewright; J. of Heat Transfer, p.1, Transactions of ASME (February 1968).

24. Daly and Pracht; Phys. of Fluids 11(1), 15 (1968).

25. Data from Bayley, Owen and Turner; Heat Transfer, Table A8 (1972).

26. See e.g., Dennery and Krzywicki; Mathematics for Physicists (Harper & Row, 1967), pp.334-346.

27. a) Gosman, Pun, Runchal, Spalding and Wolfshtein; Heat and Mass Transfer in Recirculating Flows (Academic Press, 1969).
b) Patankar and Spalding; Int'l. J. of Heat Mass Transfer 15, 1787-1806 (1972).

28. Aziz and Hellums; Phys. of Fluids 10(2), 314-324 (1967).

29. See e.g., Harlow and Welch, Phys. of Fluids 8, 2182-2189 (1965).

30. Chorin; Math. Computation 22, 745 (1968).

31. Piacsek and Williams; J. Comput. Phys. 6, 392-405 (1970).

32. Deardorff; J. Fluid Mech. 41, 453 (1970).

33. Thommen; Zeits. fur Ang. Math. und Phys. 17, 369-384 (1966).

34. As a rare example, see: Zuber; Monographs and Memoranda No. 12, Staatliche Forschungs Institute fur Maschinenbau, Bechovice, Czechoslovakia (1972).

35. a) Patankar and Spalding; Imperial College, Mechanical Engineering Dept. Report EF/TN/A/46 (June 1972).

b) Pai, Michelfelder and Spalding; Int. J. of Heat and Mass Transfer 21, 571-580 (1978).

36. Roache; Computational Fluid Dynamics (Hermosa Publishers, 1976), p.174.

37. See e.g., Coretto, Gosman, Patankar and Spalding; Lecture Notes in Physics, No.19, p.60 (Springer-Verglag, 1973).

38. Raithby and Torrance; Comput. Fluids 2, 191 (1974).

39. Runchal; Int. J. Num. Methods in Eng. 4, 541-550 (1972).

40. Roache, Computational Fluid Dynamics (Hermosa Publishers, 1976), p,32.

41. Torrance, Davis, Eike, Gill, Gutman, Hsui, Lyons and Zien; J. Fluid Mechanics 51, part 2, 221-231 (1972).

42. Carnahan, Luther and Wilkes; Applied Numerical Methods (John Wiley & Sons, 1969), p.302.

43. Peaceman and Rachford; J. Soc. Industr. Appl. Math. 3, 28-41 (1955).

44. Donovan; AIAA Jour. 8(3), 524-529 (March 1970).

45. de Vahl Davis; Int. J. of Heat and Mass Transfer 11, 1675-1693 (1969).

46. de Vahl Davis and Thomas; Phys. Fluids Supply II, 12, II-198 (1969).

47. Emery; J. Heat Transfer (Trans. ASME) 11, 1675 (1963).

48. Portier and Arnas; in Proceedings of International Centre for Heat Mass Transfer, Dubrovnik, Yugoslavia, August 1976 (Hemisphere Publishing, 1977), pp.797-806.

49. Burnay, Hannay and Portier; in Proceedings of International Centre for Heat Mass Transfer, Dubrovnik, Yugoslavia, August 1976 (Hemisphere Publishing, 1977), pp.807-811.

50. Rubel and Landis; Phys. Fluids Suppl. II, 12, II-208 (1969).

51. Quon; Phys. of Fluids 15(1), 12-19 (January 1972).

52. Fromm; in NBS Building Science Series No. 39, 451-464 (1971).

53. Kreith; Principles of Heat Transfer (Intext Press, 1973).

54. Ruberg; M.S. Thesis, Massachusetts Institute of Technology (1978).

APPENDIX A:
MORE ON DIFFERENT SCHEMES

As discussed in Chapter 3, the method of differencing (i.e., putting a differential equation into finite difference form) and the iterative scheme employed to solve the particular set of difference equations are two distinct steps in solving the problem. Here we are considering only the differencing schemes and their weak and strong points.

Consider the one-dimensional simple conduction-convection problem. Since the problem is one-dimensional, ordinary differential equations suffice and have exact analytical solutions. One can visualize the behavior of simple analytical functions and gain an intuitive feel for the character of the solutions in this situation. Also, this method will bring out more clearly some of the advantages and limitations of the numerical scheme considered here.

Given the flow field (i.e., the velocity and density at all grid nodes), one would like to compute the temperature field. The equation for temperature is:

$$\frac{\partial}{\partial t}(\rho\theta) + \frac{\partial}{\partial x}(\rho u\theta) = \frac{\partial}{\partial x}\left(\Gamma \frac{\partial \theta}{\partial x}\right) \quad . \tag{A-1}$$

Further limiting the problem to the steady-state, then u, ρ and θ are functions of x only. Equation (A-1) becomes

$$\frac{d}{dx}(\rho u\theta) = \frac{d}{dx}\left(\Gamma \frac{d\theta}{dx}\right) \quad . \tag{A-2}$$

Also, the continuity equation gives

$$\frac{d}{dx}(\rho u) = 0 \qquad \text{or} \qquad \rho u = \text{constant} \quad . \qquad \text{(A-3)}$$

Consider Fig. A-1. W, P, E, etc. are three consecutive nodes of this one-dimensional grid. Points e and w are midway between the nodes P and E and W and P. The one-dimensional "control volume" around the node P extends from point w to point e. Distance PE is denoted by $(\delta x)_e$; distance WP is denoted by $(\delta x)_w$.

We can integrate Eq. (A-2) over this one-dimensional control volume. The integration yields:

$$(\rho u\theta)_e - (\rho u\theta)_w = \left(\Gamma \frac{d\theta}{dx}\right)_e - \left(\Gamma \frac{d\theta}{dx}\right)_w \quad . \qquad \text{(A-4)}$$

This equation is exact. So far no assumptions or approximations have been made.

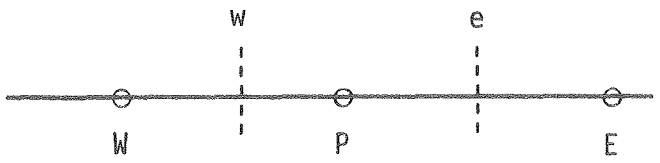

FIGURE A-1

Equation (A-4) is to be solved using finite difference approximations to the different terms in this equation. One approach would be to write

$$\left(\Gamma \frac{d\theta}{dx}\right)_e = \Gamma_e \frac{\theta_E - \theta_P}{(\delta x)_e} \quad ,$$

$$(\rho u\theta)_e = (\rho u)_e \frac{\theta_E + \theta_P}{2} \quad ,$$

(see Fig. A-1) and similarly for point w; we substitute into Eq. (A-4) and obtain an equation for θ_P of the form

$$a_P\theta_P = a_E\theta_E + a_W\theta_W \quad ,$$

where

$$\begin{aligned} a_E &= D_e - C_e/2 \\ a_W &= D_W + C_W/2 \\ a_P &= a_E + a_W \\ D_e &= \Gamma/(\delta x)_e \qquad \text{(the diffusion term)} \\ C_e &= (\rho u)_e \qquad \text{(the convection term)} \end{aligned} \tag{A-5}$$

and similar definitions hold for D_W and C_W. The staggered grid system described in Chapter 3 is assumed.

This discretized form of Eq. (A-2) is based on an assumption of linear variation of θ and neighboring grid nodes. Since some assumption about the value of θ midway between P and E must be made, the arithmetic mean of θ_P and θ_E which first comes to mind is the simplest (and the most simple-minded) assumption.

The scheme characterized in Eqs. (A-5) is known as the central difference scheme (CDS).

Equation (A-5) will now be used to compute θ_p. Suppose in a given problem one has calculated $D_e = D_w = 2$ and $C_e = C_w = 8$. Suppose also that the values of temperature at E and W have been calculated and they are to be used to calculate the temperature at P, taking into account the combined effects of diffusion and convection. If $\theta_E = 200$ and $\theta_W = 100$, we obtain $\theta_p = 50$, i.e., the temperature at P is below the temperatures at E and W. A clearly unrealistic result in the steady-state with no temperature sources and sinks. If instead, $\theta_E = 100$ and $\theta_W = 200$, one obtains $\theta_p = 250$, an equally inadmissable result. The unrealistic results arise because the coefficients in Eq. (A-5) are not all positive. For the particular values of C and D selected for this example,

$$a_E = D_e - \frac{C_e}{2} < 0 \quad .$$

Thus the temperature at P is coupled to the temperature at E with a negative coefficient. This will happen whenever $D - C/2 < 0$ for any point, i.e., whenever $C/D < 2$.

Substituting for C and D shows that in terms of fundamental variables, one must have

$$\frac{\rho u(\delta x)}{\Gamma} < 2 \quad .$$

The quantity on the left-hand side is readily recognized as the grid Péclet number. The CDS scheme gives meaningless results for temperature (or momentum) calculations whenever the grid Péclet number (or Reynolds number) exceeds 2.

To keep the grid Péclet number less than 2, one can decrease (δx), if feasible. But often this means that the number of grid nodes then

becomes larger than the memory of any existing computer. Another method, that of artificially increasing Γ, has limitations.

This limitation of CDS led to the recognition by several independent investigators (e.g., Ref. A-1 and Ref. A-2) that this problem can be solved by abandoning the CDS approximation of the convection term, using instead a one-sided (upwind or upstream) difference scheme.

The upwind difference scheme (UDS), when applied to the one-dimensional problem discussed above, leads to the following finite difference expression for θ_P [compare with Eqs. (A-5)]:

$$a_P\theta_P = a_E\theta_E + a_W\theta_W$$

where

$$\begin{aligned} a_E &= D_e + \max[-C_e, 0] \\ a_W &= D_W + \max[C_W, 0] \\ a_P &= a_E + a_W \end{aligned} \qquad \text{(A-6)}$$

D_e, D_W, C_e, and C_W are defined as before and

$$D_X = \frac{\Gamma}{(\delta x)_X} \quad , \qquad C_X = (\rho u)_X \qquad (x = e \text{ or } w) \ .$$

On inspection, it is obvious that the coefficients a_E and a_W can never be negative, so the source of the instability is gone. Also, since $C_e = C_W$, we see that only node E or node W (of Fig. A-1) will have a convective contribution to node P (depending on the direction of the flow), and both the nodes E and W will have conductive (diffusion) contributions to node P independent of the direction and magnitude of the flow.

Equation (A-2) is an ordinary differential equation. It can be solved exactly, and will allow us to examine the behavior of the solution analytically. We have:

$$\frac{d}{dx}(\rho u\theta) = \frac{d}{dx}\,\Gamma\,\frac{d\theta}{dx} \quad ,$$

with boundary conditions set as

$$\theta = \theta_0 \qquad \text{at} \qquad x = 0$$

$$\theta = \theta_L \qquad \text{at} \qquad x = L \quad .$$

The solution is

$$\frac{\theta - \theta_0}{\theta_0 - \theta_L} = \frac{\exp(Px/L) - 1}{\exp(P) - 1} \quad , \qquad \text{(A-7)}$$

where $P = \rho uL/\Gamma$ is the Péclet number. Taking $x = 0$ as one node and $x = L$ as the next (neighboring) node, then Eq. (A-7) gives the distribution of θ as one moves from one node to the next. This distribution is strongly affected by the value of the dimensionless parameter P of the problem.

Various profiles of θ vs. x for different values of P are shown in Fig. A-2; this figure illustrates several points:

(1) The assumption that the value of θ at $x = L/2$ is simply the mean of θ_0 and θ_L is valid only for very small values of $|P|$. Recall that this was the assumption made in the derivation of Eq. (A-5), the CDS equation.

(2) When $|P|$ is large, the value of θ at $x = L/2$ is almost equal to the value of θ at the upwind node. This assumption went into Eq. (A-6), the UDS equation. But, in Eqs. (A-6), the

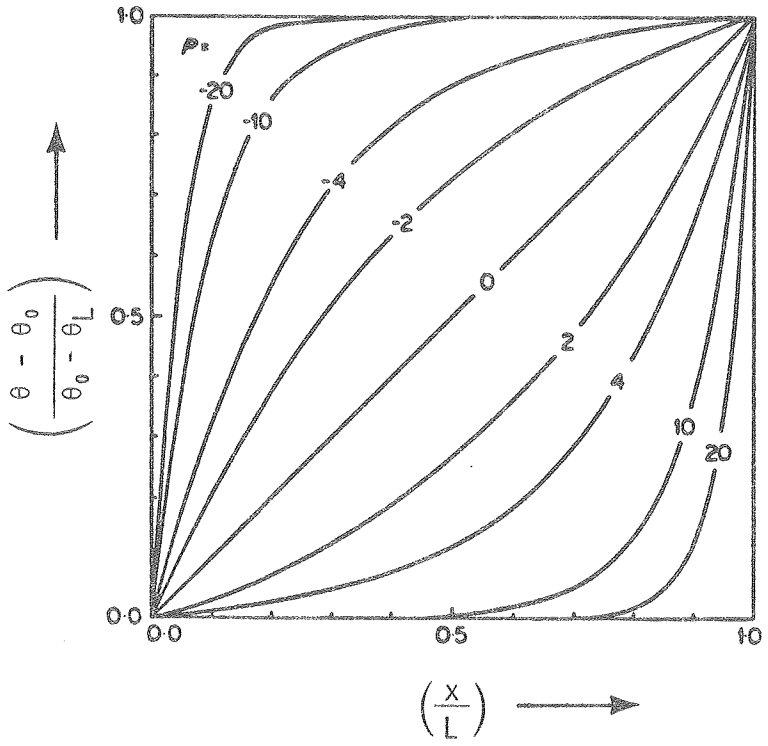
1·0
0·5
0·0
0·0
0·5
1·0
Pe
-20
-10
-4
-2
0
2
4
10
20
$\left(\frac{\theta - \theta_0}{\theta_0 - \theta_L}\right)$
$\left(\frac{X}{L}\right)$

Fig. A-2

assumption was made in the convection term that the value of θ at $x = L/2$ is always equal to the value at the upwind node, independent of the magnitude of P. This is evidently not the case.

(3) One can also see that the gradient of θ across the boundary at $x = L/2$ is simply the value used in Eqs. (A-5) and (A-6), i.e., both in CDS and UDS, in the diffusion term. But at $|P| >> 1$ the gradient is nearly zero, and therefore, so is the diffusive flux across the interface.

Finally, since there is an exact solution to this one-dimensional equation, one can use this equation to construct a difference scheme based directly on this exact solution. Then, that scheme would be correct for both convective and diffusive terms at all values of the Péclet number. Such a scheme was proposed by Raithby and Torrance in 1974 (Ref. A-3).

Spalding (Ref. A-4) proposed a fast and simplified scheme to simulate this behavior in an approximate way. In this scheme, the value of θ at L/2 [i.e., the value of θ_e in Eq. (A-4) above] depends on the value of P, the grid Péclet number. For $|P| \geq 2$, only the upwind value is assumed. For $|P| < 2$, θ_e takes on a value intermediate between θ_P and θ_E as described in Chapter 3.

REFERENCES TO APPENDIX A

A-1. Courant, Issacson and Rees; Comm. Pure Appl. Math. 5 (1952).

A-2. Torrance; J. Res. NBS 72B (1968), pp.281-301.

A-3. Raithby and Torrance; Computers & Fluids 2 (1974), p.19;

A-4. Spalding; Int. J. Num. Methods in Eng. 4 (1972), p.551.

TECHNICAL INFORMATION DEPARTMENT
LAWRENCE BERKELEY LABORATORY
UNIVERSITY OF CALIFORNIA
BERKELEY, CALIFORNIA 94720